JOURNAL OF PETROLOGY | VOLUME 49 | NUMBER 2 | PAGES 239–265 | 2008 | doi:10.1093/petrology/egm079

Ca-rich Ilvaite–Epidote–Hydrogarnet Endoskarns: a Record of Late-Magmatic Fluid Influx into the Persodic Ilímaussaq Complex, South Greenland

GESA GRASER AND GREGOR MARKL*

INSTITUT FÜR GEOWISSENSCHAFTEN, AB MINERALOGIE UND GEODYNAMIK, EBERHARD-KARLS-UNIVERSITÄT, WILHELMSTR. 56, 72074 TÜBINGEN, GERMANY

RECEIVED JUNE 26, 2006; ACCEPTED NOVEMBER 15, 2007
ADVANCE ACCESS PUBLICATION DECEMBER 26, 2007

Endoskarn assemblages involving the Ca-silicates ilvaite, epidote and Ca-rich garnet occur along fracture zones in the persodic Ilímaussaq intrusion, South Greenland. The 1·16 Ga intrusion solidified at a depth of about 3–4 km, below a cover of sandstones and pillow-basalts of the Eriksfjord Formation. In contrast to typical skarn assemblages, the Ilímaussaq endoskarns contain albite as a main phase and they did not form in metacarbonate rocks, as these are completely lacking in the vicinity of Ilímaussaq. Instead, they record late- to post-magmatic interaction of possibly external Ca-rich fluids with the alkaline to agpaitic magmatic rocks. Accordingly, endoskarn textures clearly reflect the magmatic textures of the precursor rocks. Phase relations in two endoskarn varieties with epidote + albite + andradite-rich garnet ± ilvaite ± retrograde prehnite suggest their formation at about 500°C at high oxygen fugacities slightly above the hematite–magnetite oxygen buffer [FMQ (fayalite–magnetite–quartz) + 5 to FMQ + 7] with later small modifications as a result of fluid influx or cooling of the original fluid at about 300–350°C (formation of prehnite) and at about 200–250°C (oxygen isotopic re-equilibration of the albite). One model for the formation of the observed assemblages is the decomposition of Ca-bearing minerals, such as primary eudialyte, clinopyroxene or ternary feldspar, and redistribution of the Ca by a metasomatizing late-magmatic fluid. Stable isotope (O, H) investigations, however, favour a model in which seawater was the metasomatizing fluid, which entered the Eriksfjord basalts above the intrusion, reacted with them (spilitization) and brought about 10^{-3} mol/l Ca along fractures into the metasomatized rocks. Fluid–rock interaction in the Eriksfjord basalts is documented by abundant chlorite–epidote–quartz assemblages; high fluid/rock ratios allowed the fluid to retain its seawater oxygen isotope composition.

KEY WORDS: *agpaite; endoskarn; Ilímaussaq; ilvaite; metasomatism; seawater*

INTRODUCTION

The crystallization conditions and chemical evolution of peralkaline rocks are of major interest because some of them show extreme fractionation trends with particularly long crystallization intervals between 1000 and 400°C (Sood & Edgar, 1970; Edgar & Parker, 1974; Larsen & Sørensen, 1987). Additionally, the Ivigtut cryolite deposit and extraordinary features such as rare-element pegmatites, occurrence of high field strength elements (HFSE) such as Zr, Hf, Ta or Nb, which are unusually enriched to economic levels in some peralkaline complexes, or liquid immiscibility features have long attracted the curiosity of igneous petrologists (e.g. Sørensen, 1992, 1997; Pauly & Bailey, 1999; Markl, 2001*a*; Sørensen *et al.*, 2003; Veksler, 2004). Salvi & Williams-Jones (1990, 1996) and Salvi *et al.* (2000) have shown that late-magmatic Zr enrichment is related to F-rich late-magmatic to hydrothermal HFSE-rich fluid phases and the deposition of Ca-rich Zr-silicates. Importantly, Salvi & Williams-Jones (1990, 2006) and Salvi *et al.* (2000) showed that late-stage fluids not only mobilize

*Corresponding author. E-mail: markl@uni-tuebingen.de

© The Author 2007. Published by Oxford University Press. All rights reserved. For Permissions, please e-mail: journals.permissions@oxfordjournals.org

Downloaded from https://academic.oup.com/petrology/article/49/2/239/1551155 by guest on 20 April 2024

elements, but may also redeposit and thereby concentrate them to economic levels. Therefore, the chemical evolution of late-magmatic to hydrothermal fluids, unusual Ca-rich assemblages and fluid–rock interaction processes in peralkaline intrusions are of interest for igneous petrologists, geochemists and economic geologists.

The Ilímaussaq intrusion is of particular interest in all of these respects, as it is a textbook example of a peralkaline complex (Larsen & Sørensen, 1987; Markl *et al.*, 2001; Sørensen, 2001), offers major challenges to the understanding of the geochemical evolution of magmas (Stevenson *et al.*, 1997; Marks *et al.*, 2004), and hosts one of the major Zr, Nb, Ta and rare earth element (REE) deposits of the world (Bohse *et al.*, 1971; Sørensen, 1992).

Late-stage phenomena in this intrusion include Be-rich hydrothermal veins (Engell *et al.*, 1971; Markl, 2001*b*) and immiscibility features involving extremely Th-, Nb- and REE-rich residual melts (Markl, 2001*a*). Different varieties of late-stage veins have allowed quantitative reconstruction of the pH evolution of hydrothermal fluids (Markl & Baumgartner, 2001; Sørensen *et al.*, 2003) and the enrichment of Na in the last magmatic to hydrothermal stages (Sørensen, 1962; Engell *et al.*, 1971; Schönenberger *et al.*, 2006; Müller-Lorch *et al.*, 2007).

An interesting and hitherto little studied late-stage phenomenon is Ca-rich mineral assemblages containing Ca-garnet, epidote and ilvaite (Ussing, 1912; Petersen *et al.*, 1995), which are typically known from skarn assemblages in contact metamorphic carbonates (Einaudi *et al.*, 1981; Einaudi & Burt, 1982; Meinert *et al.*, 2005). Examples of skarn assemblages with no relation to carbonate rocks are scarce. One is the Sasano copper skarn, Yoshioka Mine, Japan, which is believed to have formed from aluminous sedimentary rocks by the interaction with Ca- and Fe-rich hydrothermal solutions (Shimazaki, 1982). As carbonate rocks are absent in the vicinity of the Ilímaussaq complex, these endoskarn assemblages, which are unusual for a persodic intrusion, can be used to understand quantitatively the late-stage metasomatic interaction of the intrusion with fluids and the physico-chemical conditions during this interaction.

GEOLOGICAL SETTING

The 1·16 Ga Ilímaussaq intrusive complex is part of the mid-Proterozoic (1·1–1·3 Ga) Gardar failed rift province in South Greenland (Upton & Emeleus, 1987; Krumrei *et al.*, 2006). During this period, 10 major and several minor alkaline complexes intruded the early Proterozoic Ketilidian basement (Garde *et al.*, 2002; Upton *et al.*, 2003). The emplacement depth of the Ilímaussaq intrusion is estimated at 3–4 km (equivalent to 1 kbar; Konnerup-Madsen & Rose Hansen, 1984), close to the contact of the basement granites with the sandstones and basalts of the Eriksfjord Formation, which overlie the basement unconformably (Poulsen, 1964).

The rocks of the Ilímaussaq intrusion show a strong fractionation trend of the parental alkaline magma. Four magma batches intruded successively (Sørensen *et al.*, 2006; Krumrei *et al.*, 2007), producing first a barely silica-saturated augite syenite, in the second stage a peralkaline granite, and finally two sets of silica-undersaturated agpaitic nepheline syenites (Fig. 1). The agpaites form the major part of the intrusion and are divided into sodalite foyaite and naujaite of stage three, and the layered kakortokites and the lujavrites of stage four. All of these agpaitic rocks are different-textured varieties of nepheline or sodalite syenite. The agpaitic rocks in the southern part of the intrusion are separated from the augite syenite by an up to 100 m thick marginal pegmatite comprising pegmatitic veins in an agpaitic matrix (Bohse *et al.*, 1971; Sørensen, 2006; Fig. 2a). Mineralogically, it is similar to the kakortokites, but in parts is much coarser and texturally extremely heterogeneous (Bohse *et al.*, 1971). Andersen *et al.* (1988) and Petersen *et al.* (1995) described occurrences of this marginal pegmatite on the north coast of the Kangerluarsuk fjord and on the south coast of the Tunulliarfik fjord (Fig. 1). Sørensen (2006) gave a detailed overview of the various outcrops of marginal pegmatite.

The crystallization temperatures in the intrusion range from ~900°C to ~450°C (Sørensen, 1969; Piotrowski & Edgar, 1970; Markl *et al.*, 2001), indicating an extraordinarily long crystallization interval (Sood & Edgar, 1970; Larsen, 1976; Edgar & Parker, 1974; Larsen & Sørensen, 1987). During magmatic differentiation, the oxygen fugacity (fO_2) in the augite syenite decreased from FMQ − 1 (where FMQ is fayalite–magnetite–quartz) to below FMQ − 4, but increased during further differentiation and cooling in the agpaitic stage to FMQ + 2 to FMQ + 4 (Markl *et al.*, 2001). Crystallization in a closed system is believed to be responsible for this peculiar redox trend (Markl *et al.*, 2001).

Late-magmatic to hydrothermal veins are present in all Ilímaussaq rock types and consist mostly of aegirine, albite, sodalite, analcime, and rare minerals such as ussingite ($Na_2AlSi_3O_8OH$) or Be-silicates (Engell *et al.*, 1971; Markl, 2001*b*). Some of these veins formed by fluid–rock interaction between the Ilímaussaq rocks and an autometasomatic hydrothermal fluid rich in Na (Markl & Baumgartner, 2001). Fluid inclusion data and phase equilibria indicate formation temperatures between 300 and 400°C for these veins (Sobolev *et al.*, 1970; Konnerup-Madsen & Rose-Hansen, 1982; Markl, 2001*b*).

Early workers including Lorenzen (1881), Bøggild (1902) and Ussing (1912) mentioned the presence of ilvaite [$CaFe^{3+}(Fe^{2+})_2O(Si_2O_7)(OH)$] in the Ilímaussaq intrusion. Although the presence of ilvaite without quartz is unusual (Bartholomé & Dimanche, 1967), the Ilímaussaq

Downloaded from https://academic.oup.com/petrology/article/49/2/239/1551155 by guest on 20 April 2024

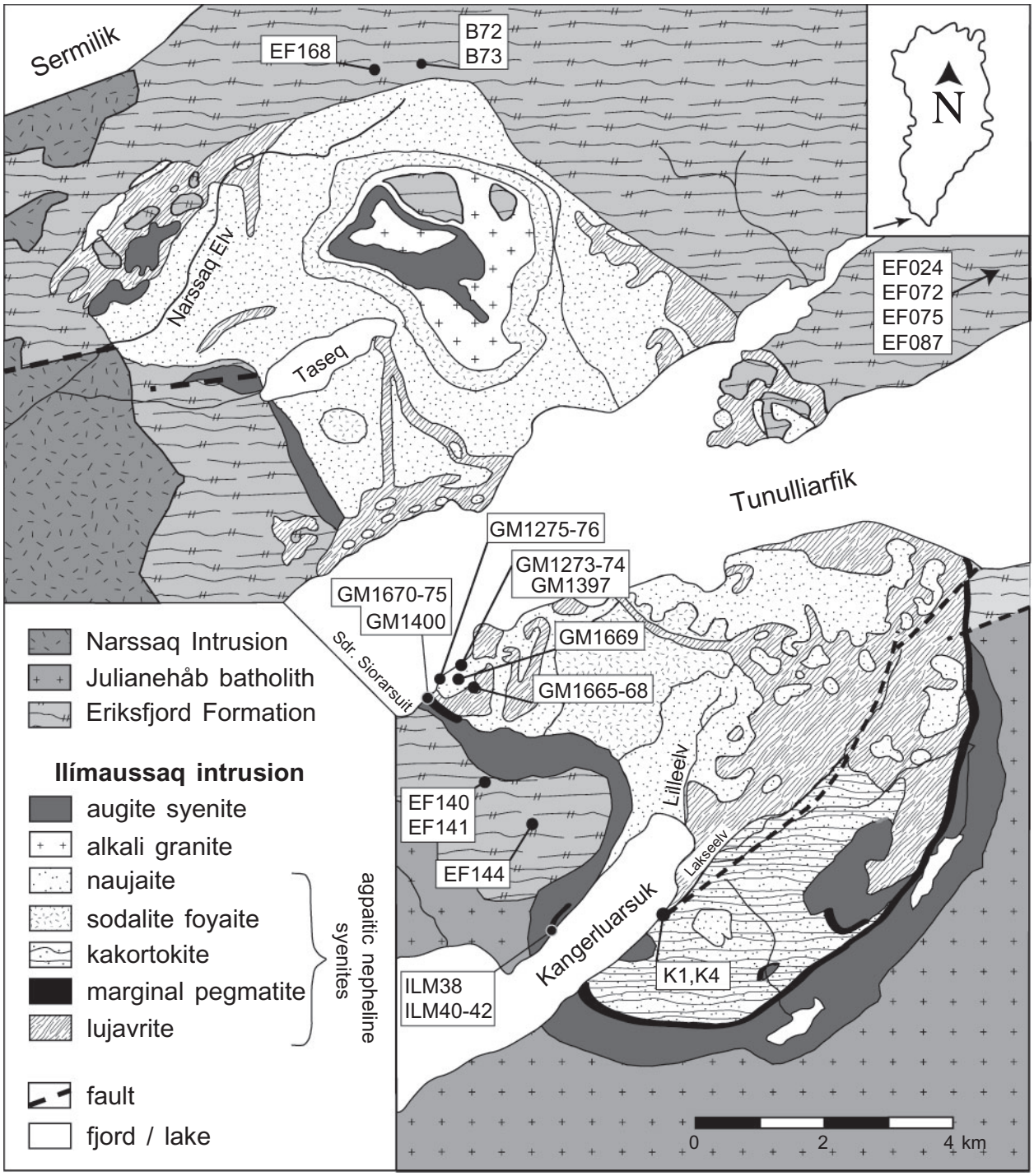

Fig. 1. Geological map of the Ilímaussaq intrusion (after Ferguson, 1964; Anderson *et al.*, 1988) with sample locations.

ilvaite and its mode of formation has not been studied in detail yet. Ferguson (1964) reported the occurrence of ilvaite associated with grossular and interpreted its formation as the result of conversion of aegirine and/or arfvedsonite, but he did not explain the gain in and the source of Ca. Petersen *et al.* (1995) described bavenite [$Ca_4(Al,Be)_4Si_9O_{26}(OH)_2$] from the Ilímaussaq ilvaite-bearing assemblage and noted that the ilvaite occurrences belong to a zone of pneumatolytic alteration mapped by Ferguson (1964). This zone comprises parts of the nepheline

Downloaded from https://academic.oup.com/petrology/article/49/2/239/1551155 by guest on 20 April 2024

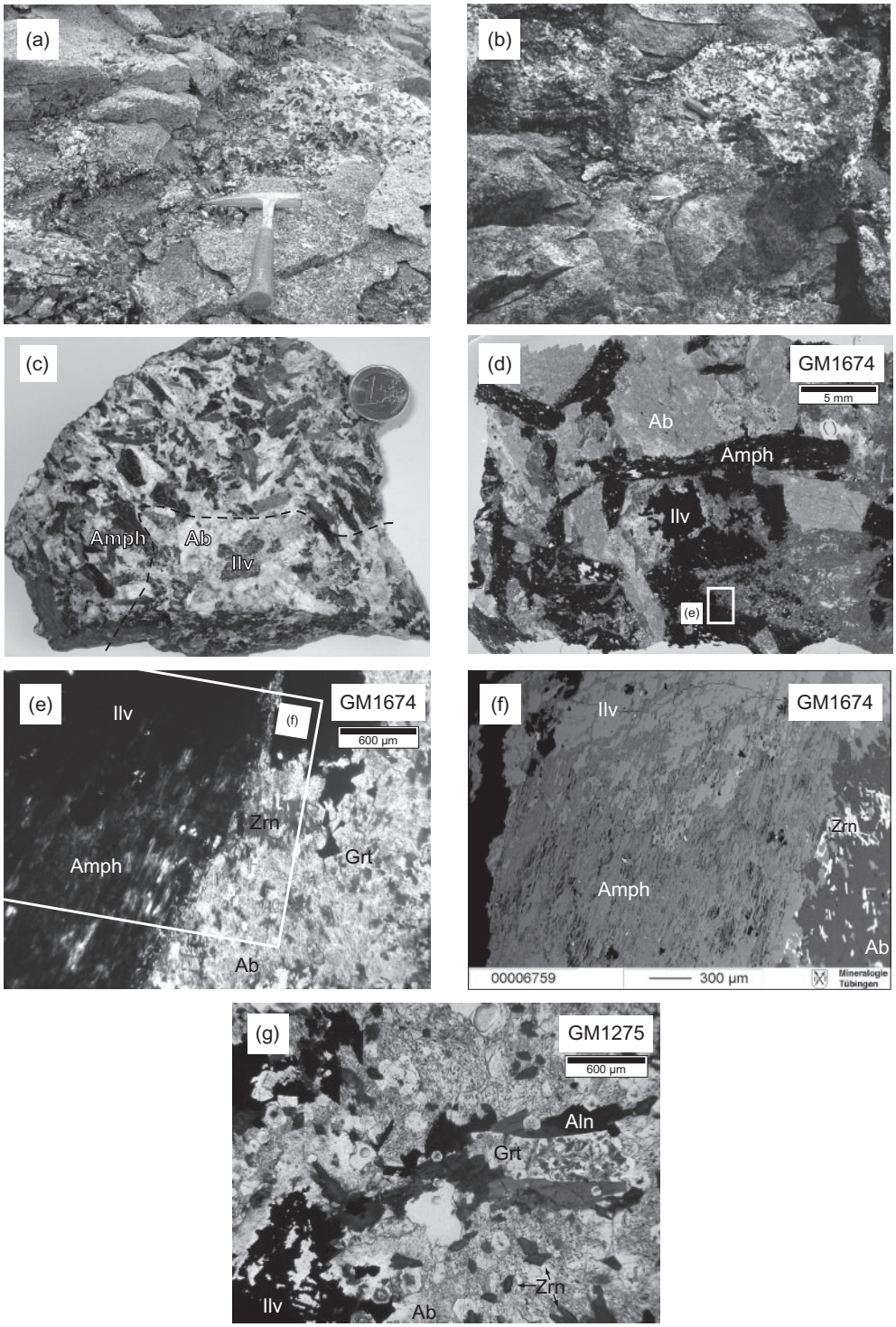

Fig. 2. Textures of the unaltered marginal pegmatite and of the ilvaite-bearing assemblage. (a) Outcrop photograph of the marginal pegmatite at Sdr. Siorarsuit. Pegmatitic vein (upper right side to lower left side) and matrix are clearly distinguishable. Photograph courtesy of H. Sørensen. (b) The pegmatitic ilvaite-bearing assemblage (upper part of the photograph) in the fine-grained, ilvaite-free matrix (lower part) at the south coast of the Tunulliarfik fjord. The Swiss army knife above the centre indicates scale. (c) Specimen with ilvaite and amphibole. The dashed line indicates the alteration front from amphibole to ilvaite. (d) Thin section of GM1674 with dark minerals (ilvaite and amphibole), light grey feldspar and grey hydrogarnet. (e) The enlargement of the section marked in (d) with a box shows on the left side alteration from amphibole to ilvaite. Hydrogarnet and zircon occur between the albite grains on the right side of the thin section. (f) BSE image of amphibole (bottom) reacting to ilvaite (top) from the box section in (e). The bright needles on the lower right are zircons. (g) REE-rich epidote to allanite enclosed by hydrogarnet and spindle-shaped zircon in sample GM1275.

Downloaded from https://academic.oup.com/petrology/article/49/2/239/1551155 by guest on 20 April 2024

syenites, the augite syenite and the marginal pegmatite (Ferguson, 1964; Petersen *et al.*, 1995).

FIELD OBSERVATIONS

Endoskarns were investigated in two areas in the southern part of the intrusion at its western margins (Fig. 1): on the south coast of the Tunulliarfik fjord and along the coast of the Kangerluarsuk fjord. Ilvaite was found at two localities associated with the marginal pegmatite (samples GM1273, GM1275, GM1276, GM1400, GM1670–GM1675 and ILM38 and ILM40–ILM42). All other endoskarns are free of ilvaite and are, based on field relations and petrography, interpreted as altered naujaites (sample GM1274, GM1397, GM1666–GM1667 and GM1669), altered foyaite (GM1665), and altered augite syenite (GM1668). A small locality on Kangerluarsuk's south coast within the kakortokites close to the major fault zone through the Lakseelv valley comprises similarly altered rocks (K1, K4) with naujaitic textures, although unaltered naujaite is not known from this locality. An ilvaite-bearing locality in the Lakseelv valley mentioned by Bohse *et al*. (1971) was not sampled during the present study. In general, ilvaite in Ilímaussaq is found only where augite syenite and marginal pegmatite have been exposed to secondary alteration (H. Sørensen, personal communication).

Ussing (1912) described the field relations of the ilvaite locality on the south coast of Tunulliarfik. Here, the rocks have been intensely altered over an area of about a quarter of a square kilometre and the pristine mineralogical composition of augite syenite, naujaite, lujavrite, and marginal pegmatite is partially or wholly replaced. Ussing (1912) interpreted the alteration as the result of 'pneumatolytical action' of varying intensity. Thus, the alteration in this region, which is responsible for the endoskarn formation with or without ilvaite, not only affects different rock types, but also is of variable intensity. The suite of newly formed minerals identified by Ussing (1912) comprises epidote, garnet, hematite, fluorite, well-crystallized albite, and ilvaite.

Both altered augite syenite and the pegmatitic veins on the north coast of Kangerluarsuk contain amongst others ilvaite and green garnet (Ussing, 1912). Petersen *et al*. (1995) studied bavenite from this ilvaite occurrence and also described calcite and a Na-zeolite.

The ilvaite-bearing rocks we studied are very heterogeneous in texture and mineral distribution and thereby perfectly reflect the texture of the mixed zone of pegmatite veins and agpaitic rocks referred to as the marginal pegmatite (Fig. 2a and b; Bohse *et al.*, 1971). In these areas ilvaite occurs mainly as large crystals (up to 3 cm) in the pegmatitic parts of the rocks (Fig. 2b and c), whereas the finer-grained rocks lack ilvaite. The precursor rocks to the finer-grained parts must have been richer in eudialyte and poorer in amphibole. The coarse-grained rocks show vugs up to several millimetres in size lined by euhedral crystals of ilvaite, garnet, epidote or albite.

The ilvaite-free epidote-bearing assemblages south of the Tunulliarfik fjord occur within augite syenite, naujaite, and foyaite close to the ilvaite-bearing rocks. Except for the lack of ilvaite, they are similar mineralogically. Fresh rocks could be sampled only along the coast, but the endoskarn assemblage also occurs in boulders further inland. The typical textures of the precursor rock types (e.g. naujaite) are commonly preserved, but original mineral grains are now pseudomorphed by fine-grained mineral assemblages.

PETROGRAPHY

Ilvaite-bearing assemblage

Black, lustrous ilvaite occurs as millimetre- to centimetre-sized subhedral lath-like crystals and is intergrown with small crystals of albite or potassium feldspar and more rarely with garnet, epidote and aegirine. In places, ilvaite may have a dendritic shape, and it commonly replaces other minerals, mainly large amphiboles (Fig. 2c–f).

Macroscopically, amphibole is green to brown and up to 5 cm long. A conversion reaction to ilvaite is common (Fig. 2b–f). Lamellae of secondary, pleochroic olive– to brown–green or blue–green amphiboles are intergrown with albite, tracing the former shape of the primary magmatic amphibole.

The light green anhedral grains of epidote are typically smaller than 1 mm. They are intergrown with ilvaite or associated with garnet and zircon. REE-rich varieties may reach the proper allanite composition. The green to brown pleochroic allanite lamellae or grains occur together with epidote, garnet and zircon (Fig. 2g). Epidote and REE-rich epidote–allanite occur as separate phases next to each other, but also as zoned grains with variable amounts of REE.

Garnet occurs as small (usually <0·5 mm) green, euhedral grains or anhedral masses. Some of the grains are zoned with a greenish or inclusion-rich core and a colourless rim. The inclusions comprise zircon and other minerals, which are too small for identification. The garnet shows anomalous birefringence with a sector-zoned extinction caused by a minor hydrogrossular component (Rossman & Aines, 1986).

Pyroxenes are rare and occur as small relict grains overgrown by ilvaite or as fine greenish needles in albite. In both cases the pyroxenes are only a few micrometres long. In a few samples only, green to brownish pleochroic felt-like chlorite is intergrown with feldspar and/or ilvaite.

The matrix of these rocks consists mainly of white to greyish or pinkish pure albite (Fig. 2c–f), which commonly contains clusters of very small but empty inclusions, rarely small needles of aegirine and even more rarely titanite. Only back-scattered electron (BSE) images revealed the

Downloaded from https://academic.oup.com/petrology/article/49/2/239/1551155 by guest on 20 April 2024

presence of potassium feldspar as irregularly shaped zones in albite, which are less clouded by inclusions than albite. Potassium feldspar also occurs as grains along skeleton-like margins of ilvaite.

Zircon is a very common constituent in all samples (Fig. 2e and f). It occurs as small euhedral grains distributed throughout the rock. It is associated with garnet and/or epidote–allanite. Hematite is found as very small grains in albite. Titanite, violet fluorite and bavenite are rare accessories. Petersen *et al.* (1995) also described zeolites, calcite and REE-bearing minerals such as cerite-(Ce).

Ilvaite-free assemblage

Although the samples of the ilvaite-free assemblage are from two different localities they are very similar in their mineralogical composition and resemble in part the ilvaite-bearing rocks. The composition and appearance of feldspar in the matrix is similar to that of the feldspar from the ilvaite-bearing assemblage. In some samples, sericitization of feldspar is common. The pure albite is grey to whitish or pinkish if altered. Greenish epidote, albite, potassium feldspar and later prehnite replace former sodalite crystals (Fig. 3a and b). Prehnite was described previously from the southern part of the intrusion by Metcalf-Johansen (1983), forming spherulitic incrustations. In our samples, it occurs in irregular patches as a rock-forming mineral. It is restricted to some samples and occurs only in patches that almost exclusively consist of prehnite. It appears to overgrow earlier pure albite crystals. Epidote forms bars up to 1 mm in length intimately intergrown with all other minerals. Garnet is very similar to that in the ilvaite-bearing assemblage, showing anomalous birefringence with a sector-zoned extinction. It is associated with epidote, allanite, chlorite, zircon or fluorite and replaces former interstitial eudialyte. Allanite, chlorite and zircon appear as described previously in the ilvaite-bearing rocks, but chlorite as an alteration product of arfvedsonite is more common and is in places intergrown with feldspar, epidote, fluorite, garnet and/or zircon (Fig. 3c). Fluorite may be colourless and occurs as rounded grains of up to 1 mm in size. Amphibole is absent in the ilvaite-free samples. Characteristic of most ilvaite-free samples is the still clearly visible macroscopic naujaitic texture.

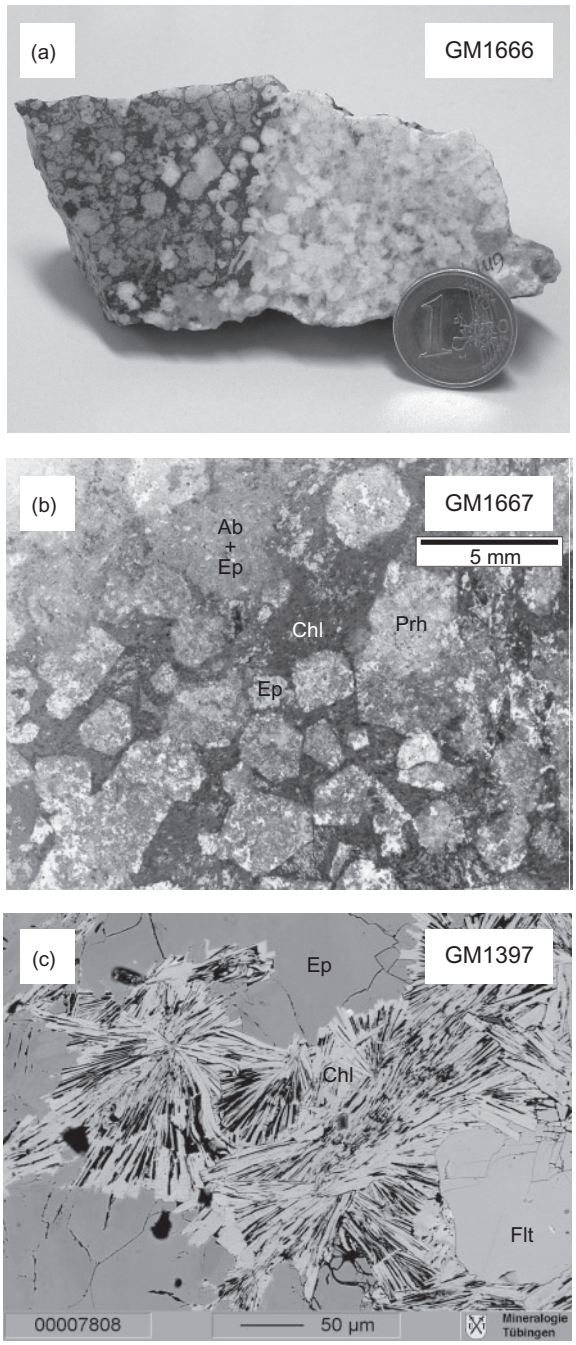

Fig. 3. Naujaite-like textures of ilvaite-free assemblages in hand specimen of sample GM1666 (a) and thin section of GM1667 (b). The left part of the hand specimen in (a) is rich in dark-coloured chlorite and epidote, whereas the right part is rich in light-coloured prehnite and feldspar. (c) Fluorite in chlorite surrounded by epidote in sample GM1397; BSE image.

ANALYTICAL METHODS

Mineral compositions were analysed using a JEOL 8900 electron microprobe at the Institut für Geowissenschaften, Universität Tübingen. Natural and synthetic standards were used for calibration. The beam current was 15 nA and acceleration voltage was 15 kV for all minerals except epidote, for which 40 nA and 20 kV were used. The measurements were performed with a focused electron beam. Counting time on the peak was 16 s for major elements and 30–120 s for minor elements. Background counting times were half the peak counting time. The raw data were corrected using the internal $\phi\rho Z$ procedures of JEOL (Armstrong, 1991). The detection limits and the typical average standard deviations (1σ) for each element

Downloaded from https://academic.oup.com/petrology/article/49/2/239/1551155 by guest on 20 April 2024

depend on the error based on count statistics. The average standard deviations govern the number of decimal places listed in Tables 1–3.

Whole-rock analyses were performed according to the methods described by Bailey *et al.* (2006). From the most homogeneous samples 1·5–2·0 kg were taken for crushing. The samples were crushed and milled in an agate mill and analysed in the laboratories of the University of Copenhagen and the Rock and Geochemistry Laboratory of the Denmark and Greenland Geological Survey using X-ray fluorescence, instrumental neutron activation analysis, inductively coupled plasma–mass spectrometry, and atomic absorption spectroscopy. These laboratories are particularly experienced in analysing rocks of such unusual bulk compositions (in terms of their minor and trace elements).

Whole-rock oxygen isotope compositions were analysed according to a modified version of the conventional method of Clayton & Mayeda (1963) and Vennemann & Smith (1990) with BrF_5 as reagent and the conversion of oxygen to CO_2 before loading into the mass spectrometer. Mineral separates were analysed using a method adapted from Sharp (1990) and Rumble & Hoering (1994) as described by Marks *et al.* (2003). NBS-28 quartz and UWG-2 garnet (Valley *et al.*, 1995) were used as standards.

Hydrogen isotope data were obtained using the method of Vennemann & O'Neil (1993) for the quantitative conversion of H_2O to H_2 from minerals and whole-rocks on a Zn reagent (University of Indiana). An internal laboratory standard (kaolinite 17, $\delta D = -125‰$) was used for calibration.

Oxygen and hydrogen isotopic compositions of minerals and whole-rocks were measured on a Finnigan MAT 252 isotope ratio mass spectrometer at the Universität Tübingen. The results are in δ-notation in permil (‰) relative to Vienna Standard Mean Ocean Water (VSMOW). The analytical precision is about ±0·2‰ for $\delta^{18}O$ and about ±2‰ for δD.

Different ilvaite-bearing and ilvaite-free whole-rock samples and hand-picked separates of ilvaite, garnet, epidote and albite of the ilvaite-bearing assemblage were analysed for their stable isotope compositions. The ilvaite-free assemblage is much finer grained, which made it impossible to separate enough pure material of single minerals. For comparison, two augite syenite whole-rock samples (GM1330, GM1857), some whole-rock Eriksfjord basalts in different degrees of alteration–from fresh (EF024, EF072, EF168) to epidotized (EF075, EF087, EF140, EF141, EF144)–and two grains of epidote from cavities in the Eriksfjord basalts (B72, B73) were also analysed (Fig. 1).

RESULTS

Mineral compositions

Ilvaite-bearing assemblage

Feldspar is commonly pure albite or, in smaller amounts, pure potassium feldspar.

Table 1 shows representative microprobe analyses of ilvaite. It may contain up to 4·2 wt % MnO, corresponding to 0·25 atoms per formula unit (a.p.f.u.). Minor elements are Na_2O (<0·42 wt %), MgO (<0·1 wt %), Al_2O_3 (0·01–1·2 wt %) and K_2O (<0·18 wt %).

Representative epidote analyses (Table 2, Fig. 4) indicate a solid solution between epidote and allanite with up to 22·4 wt % $LREE_2O_3$ ($La_2O_3 + Ce_2O_3 + Nd_2O_3$ are the predominant REE_2O_3 in the studied samples). The name allanite is used if REE are dominant on the A2 site (Gieré & Sorensen, 2004). Analyses with more than 3 wt % $LREE_2O_3$ but less than 0·5 REE a.p.f.u. are referred to as REE-rich epidote.

The garnets are almost pure granditic garnets with variable H_2O (≤2·0 wt %) and F (≤1·9 wt %) contents (Valley *et al.*, 1983; Lager *et al.*, 1989; Fig. 5). They vary in composition between Adr_{44} and Adr_{100} (Table 3, Fig. 5), and their spessartine component is ≤3 mol%. BSE images commonly show concentric or patchy zonation as a result of variable contents of Al and Fe^{3+}.

Microprobe work allows us to distinguish two types of secondary amphibole, which are, however, texturally identical: arfvedsonite to ferric-ferronyböite and potassic-hastingsite to potassic-ferritaramite (Leake *et al.*, 1997, 2004, Table 1). The ferric-ferronyböites contain about 1·15 wt % F, whereas the other sodic amphiboles have less than 1 wt %. The F content of the calcium amphiboles is close to the detection limit.

The only clinopyroxene present is aegirine (Aeg, Table 1) with compositions between $Aeg_{84}Jd_9QUAD_7$ and $Aeg_{93}Jd_5QUAD_2$ (the QUAD-component comprises enstatite, ferrosilite, diopside, and hedenbergite). The aegirine may contain up to about 1 wt % Al_2O_3, 0·106–0·214 wt % MnO, and 0·14–0·9 wt % ZrO_2.

In the ilvaite-bearing samples chlorite is Fe-rich chamosite ($X_{Mg} = 0·01–0·29$; Fig. 6, Table 1) with the average composition $chamosite_{82}clinochlore_{16}pennantite_2$.

Ilvaite-free assemblage

Feldspar occurs as pure albite and pure potassium feldspar.

Representative analyses of epidote and allanite (Table 2, Fig. 4) show a solid solution between epidote and allanite with up to 22·8 wt % $LREE_2O_3$ ($La_2O_3 + Ce_2O_3 + Nd_2O_3$).

The garnets are richer in Al and poorer in Fe^{3+} than in the ilvaite-bearing assemblage and vary between Adr_{01} and Adr_{52} (Table 3, Fig. 5). They contain up to 5 wt % F and commonly less than 2 wt % H_2O (calc.).

In the ilvaite-free samples, chlorite is a chamosite with a lower average X_{Mg} (range 0–0·35) than in the ilvaite-bearing assemblage (Fig. 6) and with the average composition $chamosite_{93}clinochlore_4pennantite_3$.

Prehnite is close to the pure end-member composition (Table 3).

Downloaded from https://academic.oup.com/petrology/article/49/2/239/1551155 by guest on 20 April 2024

Table 1: Electron microprobe analyses of minerals from the ilvaite-bearing assemblage

Sample no:	ILM41	GM1670	GM1670	GM1275	ILM42	GM1400	GM1400	GM1671	GM1675	GM1400	ILM42	ILM42	GM1670	GM1670	GM1672
Mineral:	ilvaite	Ilvaite	ilvaite	arfvedsonite	arfvedsonite	arfvedsonite/ ferric-ferronyböite	potassic-ferritaramite	potassic-ferritaramite	potassic-hastingsite	aegirine	aegirine	aegirine	chlorite	chlorite	chlorite
wt %															
SiO_2	29·75	29·57	29·78	48·0	49·6	46·9	37·6	38·7	38·1	51·2	52·3	51·9	28·08	23·91	24·53
TiO_2	0·045	0·073	0·130	0·50	0·46	0·70	0·158	0·057	<0·02	0·419	0·417	0·376	<0·02	<0·02	0·027
Al_2O_3	0·059	0·084	0·240	2·38	1·218	2·69	10·07	10·22	9·21	0·767	1·011	0·886	15·41	18·2	16·62
FeO	51·5	47·6	50·2	33·2	33·0	33·4	32·9	33·0	33·1	28·3	28·6	28·8	36·8	45·6	47·6
MnO	0·256	4·11	1·58	0·61	0·86	0·65	0·60	0·404	0·372	0·214	0·115	0·106	1·04	0·98	0·50
MgO	<0·01	0·026	0·026	0·366	0·173	0·581	0·584	0·743	1·20	0·088	0·017	0·023	7·14	1·44	0·521
CaO	13·9	13·9	13·9	2·09	0·392	2·57	7·72	7·93	9·28	4·06	1·62	2·38	0·288	0·047	0·030
Na_2O	<0·01	0·010	<0·01	7·8	8·7	7·9	3·41	3·42	2·29	11·3	12·9	12·5	0·159	0·078	0·024
K_2O	0·014	<0·01	0·023	1·69	2·33	1·61	3·05	3·02	2·99	0·015	<0·01	0·010	0·343	0·019	0·010
ZrO_2				0·25	<0·02	0·26	0·23	0·09	<0·02	0·9	0·45	0·20	<0·02	<0·02	<0·02
Cl				<0·01	<0·01	<0·01	<0·01	<0·01	<0·01				0·036	0·054	0·014
F				0·36	0·64	1·15	0·044	0·051	0·060				<0·02	<0·02	<0·02
Total	95·5	95·4	95·9	97·2	97·4	98·4	96·4	97·6	96·6	97·3	97·4	97·2	89·3	90·3	89·9
	Based on 6 cations and 8·5 oxygens			*Based on 16 cations and 23 oxygens*						*Based on 4 cations and 6 oxygens*			*Based on 20 cations and 28 oxygens*		
Si	2·03	2·01	2·02	7·71	7·92	7·50	6·17	6·27	6·29	1·99	2·00	2·00	6·27	5·52	5·76
Al	0·01	0·01	0·02	0·45	0·23	0·51	1·95	1·95	1·79	0·03	0·04	0·04	4·05	4·95	4·60
Ti	0·00	0·00	0·01	0·06	0·06	0·08	0·02	0·01	0·00	0·01	0·01	0·01	0·00	0·00	0·00
Fe^{3+}	0·94	0·96	0·93	0·76	0·97	1·04	1·35	1·19	1·00	0·81	0·89	0·89	0·00	0·06	0·00
Mg	0·00	0·00	0·00	0·09	0·04	0·14	0·14	0·18	0·29	0·01	0·00	0·00	2·37	0·49	0·18
Fe^{2+}	1·99	1·76	1·92	3·69	3·43	3·42	3·18	3·28	3·58	0·11	0·03	0·03	6·87	8·74	9·34
Mn	0·01	0·24	0·09	0·08	0·12	0·09	0·08	0·05	0·05	0·01	0·00	0·00	0·20	0·19	0·10
Ca	1·02	1·02	1·01	0·36	0·07	0·44	1·36	1·37	1·64	0·17	0·07	0·00	0·07	0·01	0·01
Na	0·00	0·00	0·00	2·44	2·69	2·43	1·09	1·07	0·73	0·85	0·95	0·93	0·07	0·03	0·01
K	0·00	0·00	0·00	0·34	0·47	0·33	0·64	0·62	0·63	0·00	0·00	0·00	0·10	0·01	0·00
Zr				0·02	0·00	0·02	0·02	0·01	0·00	0·01	0·01	0·00	0·00	0·00	0·00
Total	6·00	6·00	6·00	16·00	16·00	16·00	16·00	16·00	16·00	4·00	4·00	4·00	20·00	20·00	20·00
Cl				0·00	0·00	0·00	0·00	0·00	0·00				0·01	0·02	0·01
F				0·18	0·32	0·58	0·02	0·03	0·03				0·00	0·00	0·00

Downloaded from https://academic.oup.com/petrology/article/49/2/239/1551155 by guest on 20 April 2024

Table 2: Electron microprobe analyses of epidotes, REE-rich epidotes and allanites of the endoskarn assemblages. Low totals may be caused by the occurrence of other REEs that were not included in the analyses

Assemblage:	ilv-bearing						ilv-free					
Sample no:	ILM42	GM1670	GM1675	ILM38	GM1670	GM1275	GM1667	GM1665	GM1669	GM1669	GM1669	K1
Mineral:	epidote	epidote	epidote	REE-rich ep	REE-rich ep	allanite	epidote	epidote	epidote	REE-rich ep	REE-rich ep	allanite
wt %												
SiO_2	36·5	36·6	36·5	34·9	33·1	31·2	37·1	37·2	38·0	35·2	35·1	33·2
TiO_2	0·082	0·065	0·023	<0·02	0·550	0·098	0·046	0·043	0·087	<0·02	0·036	0·913
Al_2O_3	18·6	19·6	21·4	19·0	11·2	9·8	22·6	20·6	24·9	20·4	20·3	17·2
FeO	17·90	15·9	12·97	15·30	23·30	20·71	12·62	15·08	10·63	13·94	13·3	13·88
MnO	<0·02	0·07	0·191	0·038	0·69	3·15	0·207	0·251	<0·02	0·106	0·135	0·21
MgO	<0·01	<0·01	<0·01	<0·01	<0·01	<0·01	<0·01	<0·01	0·010	<0·01	<0·01	0·011
CaO	21·9	22·6	22·7	18·1	15·4	12·2	22·7	22·3	23·2	19·5	18·0	13·7
Na_2O	0·030	<0·01	0·018	<0·01	0·025	<0·01	<0·01	0·024	<0·01	<0·01	0·024	0·040
K_2O	<0·01	<0·01	<0·01	<0·01	<0·01	<0·01	<0·01	<0·01	<0·01	<0·01	<0·01	0·059
La_2O_3	0·14	0·13	0·15	2·0	3·0	5·5	0·25	<0·01	<0·01	1·6	2·7	3·7
Ce_2O_3	0·44	0·34	0·27	4·3	7·1	10·4	0·30	0·022	<0·01	3·2	5·1	9·2
Nd_2O_3	0·6	0·13	0·08	1·6	2·7	3·0	0·05	<0·01	<0·01	1·0	1·5	3·0
Total	96·2	95·4	94·3	95·2	97·1	96·0	95·9	95·5	96·8	94·9	96·2	95·1
Based on 8 cations and 12·5 oxygens												
Si	3·00	3·00	3·00	3·03	3·01	3·01	3·00	3·03	3·00	2·99	3·02	3·07
Al	1·81	1·89	2·07	1·94	1·20	1·12	2·15	1·98	2·32	2·05	2·06	1·87
Ti	0·01	0·00	0·00	0·00	0·04	0·01	0·00	0·00	0·01	0·00	0·00	0·06
Fe^{3+}	1·17	1·08	0·91	0·76	1·28	1·18	0·83	0·97	0·66	0·79	0·61	0·35
Mg	0·00	0·00	0·00	0·00	0·00	0·00	0·00	0·00	0·00	0·00	0·00	0·00
Fe^{2+}	0·07	0·02	0·00	0·35	0·49	0·49	0·03	0·06	0·04	0·20	0·35	0·73
Mn	0·00	0·01	0·01	0·00	0·05	0·26	0·02	0·02	0·00	0·01	0·01	0·02
Ca	1·92	1·99	2·00	1·67	1·50	1·26	1·96	1·94	1·97	1·78	1·65	1·36
Na	0·00	0·00	0·00	0·00	0·00	0·00	0·00	0·00	0·00	0·00	0·00	0·00
K	0·00	0·00	0·00	0·00	0·00	0·00	0·00	0·00	0·00	0·00	0·00	0·00
La	0·00	0·00	0·00	0·06	0·10	0·20	0·01	0·00	0·00	0·05	0·09	0·13
Ce	0·01	0·01	0·01	0·14	0·24	0·37	0·00	0·00	0·00	0·10	0·16	0·31
Nd	0·01	0·00	0·00	0·05	0·09	0·10	0·00	0·00	0·00	0·03	0·05	0·10
Total	8·00	8·00	8·00	8·00	8·00	8·00	8·00	8·00	8·00	8·00	8·00	8·00
czo	0·00	0·00	0·07	0·00	0·00	0·00	0·15	0·00	0·32	0·05	0·06	0·00
aln	0·02	0·02	0·02	0·25	0·42	0·67	0·02	0·00	0·00	0·18	0·29	0·54
ep	0·98	0·98	0·91	0·75	0·58	0·33	0·83	1·00	0·68	0·77	0·65	0·46

Low totals may be caused by the occurrence of other REE that were not included in the analyses.

Downloaded from ... April 2024

Table 3: Electron microprobe analyses of minerals from the ilvaite-bearing and -free assemblages

Assemblage:	ilv-free							ilv-bearing					
Sample no:	K4	K1I	GM1666	K1I	GM1397	GM1666		ILM41	ILM41	GM1671	K1II	K4	GM1668
Mineral:	prehnite	prehnite	prehnite	chlorite	chlorite	chlorite		garnet	garnet	garnet	garnet	garnet	garnet
wt %													
SiO_2	43·7	43·8	44·2	24·84	23·40	23·68	SiO_2	34·3	36·1	34·7	35·6	33·07	36·3
TiO_2	<0·02	<0·02	0·027	1·74	0·053	<0·02	TiO_2	<0·02	0·484	0·474	0·240	0·020	0·617
Al_2O_3	23·7	23·1	24·1	17·2	20·0	19·0	Al_2O_3	0·146	11·3	7·2	10·2	20·0	14·0
FeO	0·051	0·997	0·302	41·1	44·5	45·8	FeO calc	0·0	0·0	0·0	0·0	0·0	0·0
MnO	0·078	0·122	<0·01	1·49	0·94	0·91	Fe_2O_3 calc	31·0	14·5	20·9	17·4	3·0	11·3
MgO	<0·01	<0·01	<0·01	0·947	0·353	0·181	MnO	0·139	0·39	0·33	0·37	0·52	0·78
CaO	26·5	26·8	26·0	1·91	0·141	<0·02	MgO	0·010	<0·01	0·024	0·016	0·013	<0·01
Na_2O	0·152	0·134	0·014	0·223	0·068	0·015	CaO	33·0	34·7	34·3	35·6	36·7	35·6
K_2O	0·012	0·015	<0·01	0·021	0·014	<0·01	ZrO_2				<0·02	<0·02	<0·02
ZrO_2	<0·02	<0·02	<0·02	0·53	<0·02	<0·02	Cl				<0·01	<0·01	<0·01
Cl	0·017	<0·01	<0·01	<0·01	0·033	0·025	F	0·276	0·350	0·764	1·480	4·32	1·370
F	<0·02	<0·02	<0·02	<0·02	<0·02	<0·02	H_2O calc·	0·51	0·53	1·02	0·89	1·88	0·69
Total	94·2	95·0	94·6	90·0	89·5	89·6	Total	99·4	98·4	99·7	101·8	99·5	100·7
	Based on 14 cations and 22 oxygens			*Based on 20 cations and 28 oxygens*				*Based on the 5 cations of the X and Y-site**					
Si	6·09	6·07	6·14	5·76	5·46	5·54	Si	2·91	2·91	2·81	2·79	2·50	2·83
Al	3·90	3·77	3·94	4·70	5·49	5·24	H/4	0·07	0·07	0·14	0·12	0·24	0·09
Ti	0·00	0·00	0·00	0·30	0·01	0·00	F/4	0·02	0·02	0·05	0·09	0·26	0·08
Fe^{3+}	0·00	0·12	0·00	0·00	0·00	0·00	Cl/4				0·00	0·00	0·00
Mg	0·00	0·00	0·00	0·33	0·12	0·06	Al	0·01	1·07	0·69	0·94	1·79	1·29
Fe^{2+}	0·01	0·00	0·04	7·97	8·67	8·96	Fe^{3+}	1·98	0·88	1·27	1·03	0·20	0·66
Mn	0·01	0·02	0·00	0·29	0·18	0·18	Ti	0·00	0·03	0·03	0·01	0·00	0·04
Ca	3·95	3·98	3·87	0·48	0·03	0·00	Zr				0·00	0·00	0·00
Na	0·04	0·04	0·01	0·10	0·03	0·01	Cr	0·00	0·00	0·00			
K	0·00	0·00	0·00	0·01	0·00	0·00	Fe^{2+}	0·00	0·00	0·00	0·00	0·00	0·00
Zr	0·00	0·00	0·00	0·06	0·00	0·00	Mg	0·00	0·00	0·00	0·00	0·00	0·00
Total	14·00	14·00	14·00	20·00	20·00	20·00	Mn	0·01	0·03	0·02	0·03	0·03	0·05
							Ca	3·00	2·99	2·99	2·99	2·98	2·96
Cl	0·00	0·00	0·00	0·00	0·01	0·01	Total	8·00	8·00	8·00	8·00	8·00	8·00
F	0·00	0·00	0·00	0·00	0·00	0·00							
							Spessartine	0	1	1	1	1	2
							Grossular	1	55	35	47	89	65
							Andradite (after Deer *et al.*, 1992)	99	44	64	52	10	33
							Hydrograndite*	7	7	14	12	24	9
							Fluorograndite*	2	2	5	9	26	8
							Grandite	91	91	81	79	50	83

*Si is assumed to be present only on the Si-site. Hydrograndite: $Ca_3(Al,Fe^{3+})_2Si_2O_8(OH)_4$, Fluorograndite: $Ca_3(Al,Fe^{3+})_2Si_2O_8F_4$

Downloaded from https://academic.oup.com/petrology/article/49/2/233/1551155 by guest on 20 April 2024

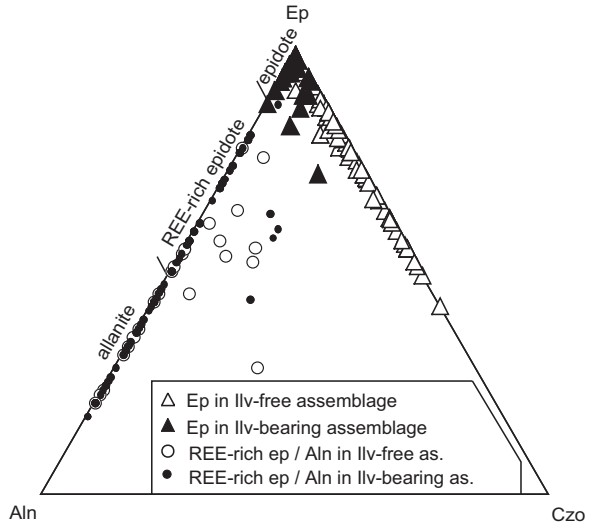

Fig. 4. Classification of the epidote-group minerals in the epidote–allanite–clinozoisite triangle. The proportion of clinozoisite was calculated as Al (a.p.f.u.) − 2 [if Al (a.p.f.u.) >2; otherwise the proportion is taken as zero], the proportion of allanite is equal to REE (a.p.f.u.), and epidote is 1 − (allanite + clinozoisite).

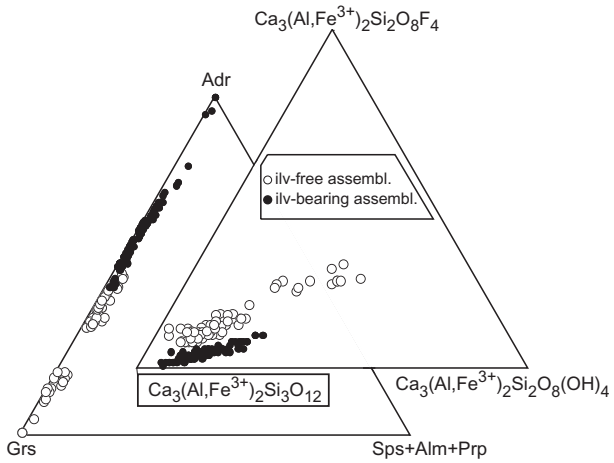

Fig. 5. Composition of the Ilímaussaq hydrogarnets in the grossular–andradite–(spessartine + almandine + pyrope) triangle and in the grandite–hydrograndite–fluorograndite triangle.

Whole-rock compositions

Five representative samples of the ilvaite-bearing assemblage and four of the ilvaite-free assemblage were selected for whole-rock analysis (Table 4). When compared with their marginal pegmatite precursor rocks (Sørensen, 2006), the ilvaite-bearing assemblages are invariably enriched in Ca. They are similar to their precursor, with small depletions in K and Al and possibly with an enrichment in Fe and Zr (Fig. 7). The peralkalinity index [P.I. = molar $(Na_2O + K_2O)/Al_2O_3$] varies between 0·83 and 0·94 (Fig. 8).

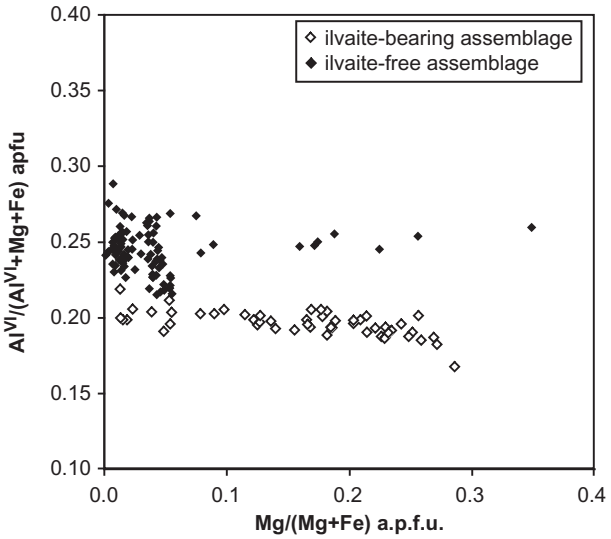

Fig. 6. Atomic ratios of Mg/(Mg + Fe) vs $Al^{VI}/(Al^{VI} + Mg + Fe)$ for chlorites in the ilvaite-bearing and ilvaite-free assemblages.

The variation in major element composition of the ilvaite-free assemblages (Table 4) is larger because of the different precursor rock types for these samples. Nevertheless, Ca is strongly enriched in GM1666 and K1 and slightly enriched in GM1668 and GM1669 with respect to their average precursor rocks (Bailey *et al.*, 2001) (Fig. 9).

Figure 10 shows a comparison of the primitive-mantle normalized trace element patterns (after McDonough & Sun, 1995) of the endoskarns, major average Ilímaussaq rock types (Bailey *et al.*, 2001) and the marginal pegmatite (Sørensen, 2006). Several trace elements in the ilvaite-bearing assemblage lie within the range of Ilímaussaq trace elements but scatter around the marginal pegmatite pattern (Fig. 10a). Interestingly, all ilvaite-bearing samples are depleted in Cs, Rb and Ba, with respect to the marginal pegmatite. The trace elements of the ilvaite-free assemblages (Fig. 10b) vary, with some exceptions, within the range of the common Ilímaussaq trace element distribution. Sample K1 is distinct in terms of its enrichment in several trace elements with respect to the other ilvaite-free samples (Fig. 10b).

Stable isotopes

The $\delta^{18}O$ values of the ilvaite-bearing whole-rock samples range between 3·0 and 6·2‰ and of the ilvaite-free assemblage between 4·5 and 6·8‰ relative to VSMOW (Table 5, Fig. 11). In the ilvaite-bearing assemblage, ilvaite values range between −4·7 and −3·6‰, garnet between −3·3 and −1·8‰, and albite between 5·9 and 7·2‰. The epidote has a value of −1·1‰. The Ilímaussaq augite syenite whole-rock samples have a $\delta^{18}O$ of 6·4 and 6·7‰, the basalts of the Eriksfjord Formation range between −1·8 and 5·5‰, and the

Downloaded from https://academic.oup.com/petrology/article/49/2/239/1551155 by guest on 20 April 2024

Table 4: XRF whole-rock analyses of skarn-like rocks in the Ilímaussaq intrusion and reference data

	ilvaite-bearing assemblage					ilvaite-free assemblage				marginal pegmatite	augite syenite (coarse)	foyaite	naujaite
Sample no:	GM1273	GM1670	GM1671	GM1674	ILM42	GM1666	GM1668	GM1669	K1	Sørensen (2006)	Bailey *et al.* (2001)	Bailey *et al.* (2001)	Bailey *et al.* (2001)
SiO_2	53·36	53·38	55·44	50·22	53·61	53·93	55·48	62·25	49·43	54·10	56·97	58·50	48·25
TiO_2	0·18	0·20	0·19	0·27	0·16	0·12	0·10	0·05	0·13	0·20	1·27	0·32	0·32
ZrO_2	1·03	0·59	1·63	0·53	3·12	0·07	0·24	0·02	2·43	1·02	0·06	0·27	0·49
Al_2O_3	14·21	12·97	14·80	11·77	14·15	20·71	18·71	19·61	18·29	15·72	16·82	16·21	19·30
Fe_2O_3	7·29	7·43	6·35	9·15	7·00	1·99	5·50	1·33	4·06	7·96	1·47	3·03	4·07
FeO	6·84	9·31	3·14	11·24	3·82	3·17	4·35	1·12	1·25	2·43	6·68	3·80	3·08
MnO	0·58	0·68	0·36	0·66	0·39	0·12	0·31	0·06	0·26	0·26	0·22	0·19	0·21
MgO	0·43	0·08	0·27	0·26	0·27	0·14	0·21	0·11	0·23	0·26	0·76	0·11	0·10
CaO	5·86	6·06	6·37	6·29	7·48	9·43	4·29	2·88	13·94	2·64	3·47	1·76	1·68
Na_2O	7·13	7·22	5·47	5·81	7·04	4·27	7·94	8·29	3·52	6·79	5·65	7·56	14·37
K_2O	0·05	0·31	3·57	1·17	0·15	3·19	0·04	2·58	2·50	4·09	5·16	5·64	3·41
P_2O_5	0·06	0·12	0·06	0·06	0·13	0·03	0·12	0·41	0·09	0·05	0·34	0·04	0·06
H_2O^+	0·93	0·90	0·72	1·39	0·71	1·51	1·71	0·47	0·81	n.r.	0·56	1·26	1·25
H_2O^-	0·16	0·07	0·05	0·07	0·17	0·05	0·33	0·07	0·04	n.r.	0·19	0·21	0·17
S	<0·01	<0·01	0·01	0·01	0·01	<0·01	<0·01	<0·01	<0·01	n.r.	0·07	0·02	0·08
Cl	0·03	0·06	0·07	0·07	0·09	0·04	0·02	0·04	0·04	0·03	0·04	0·12	2·34
F	0·06	0·09	0·16	0·06	0·10	0·25	0·06	0·04	0·45	0·23	0·14	0·20	0·16
Others	1·11	0·35	0·79	0·42	1·25	0·33	0·39	0·40	1·57	n.r.	0·06	0·17	0·01
Sum	99·32	99·80	99·46	99·45	99·62	99·35	99·80	99·72	99·04	98·71	99·98	99·45	99·55
O^-	0·03	0·05	0·09	0·05	0·07	0·11	0·03	0·03	0·20	0·11	0·1	0·12	0·65
Sum	99·29	99·75	99·37	99·40	99·56	99·24	99·77	99·69	98·85	98·60	99·88	99·33	98·9
P.I.	0·83	0·94	0·87	0·92	0·83	0·51	0·70	0·84	0·46	0·99	0·88	1·14	1·42
Cs	0·1	0·1	0·7	0·2	1·9	0·2	0·1	0·1	0·6	3·8	1·2	5·3	6·2
Rb	4·5	51	379	118	23	268	4·4	103	152	456	68	315	334
Tl	<0·5	<0·5	<0·5	0·6	<0·5	<0·5	<0·5	<0·5	<0·5	n·r·	<0·5	1·3	2·3
Ba	15	29	79	28	42	231	26	228	1282	379	2320	42	11
Pb	341	14	133	86	99	11	8	52	182	62	15	45	94
Sr	889	220	343	130	480	1171	760	1158	2866	269	395	27	10
La	1229	292	682	286	1181	119	413	327	987	541	77	244	594
Ce	2480	570	1296	539	2338	228	613	623	1846	930	163	512	1180
Pr	311	72	170	67	313	28	67	78	234	n.r.	n.r.	n·r·	n·r·
Nd	1072	259	591	233	1133	92	202	264	805	426	76	219	540
Sm	197	54·0	121	44·8	241	15·2	27·4	36·7	158	79	13·9	38·2	96·1
Eu	17·8	5·0	11·3	4·7	21·6	1·4	2·4	3·1	15·2	7·3	4·53	3·60	9·63
Gd	188	53·3	125	45·5	246	14·8	29·2	33·4	170	n.r.	n.r.	n.r.	n.r.
Tb	25·3	8·2	20·7	6·8	40·9	1·8	3·6	3·4	28·0	13·6	1·88	5·82	16·1
Dy	139	48·9	129	41·3	254	9·8	21·0	15·5	176	n.r.	n.r.	n.r.	n.r.
Ho	27·4	10·6	28·6	8·7	56·7	1·9	4·5	2·3	39·8	n.r.	n.r.	n.r.	n.r.
Er	72·6	28·5	79·9	24·4	157	5·2	13·2	5·3	113	n.r.	n.r.	n.r.	n.r.
Tm	10·2	4·4	11·8	3·7	23·3	0·7	2·0	0·6	17·0	n.r.	n.r.	n.r.	n.r.
Yb	64·7	28·9	77·7	25·3	148	5·2	13·2	3·1	110	50·2	5·30	19·7	38·3
Lu	8·4	4·1	10·4	3·7	20·0	0·8	1·8	0·4	15·0	7·0	0·80	2·43	5·24
Y	933	295	684	241	1249	64	172	62	897	471	45	184	461

(continued)

Downloaded from https://academic.oup.com/petrology/article/49/2/239/1551155 by guest on 20 April 2024

Table 4: Continued

	ilvaite-bearing assemblage					ilvaite-free assemblage				marginal	augite syenite (coarse)	foyaite	naujaite
Sample no:	GM1273	GM1670	GM1671	GM1674	ILM42	GM1666	GM1668	GM1669	K1	pegmatite Sørensen (2006)	Bailey *et al.* (2001)	Bailey *et al.* (2001)	Bailey *et al.* (2001)
Th	86	41	57	35	42	27	79	36	37	50	7·9	27·8	41·0
U	63	18	22	14	22	8	18	6	14	14	1·9	9·8	19·5
Zr	7634	4340	12073	3925	23066	552	1779	160	17973	8145	272	2070	4360
Hf	103	85·0	255	79·5	461	13·0	27·1	3·5	404	184	11·4	42·5	75·2
Nb	329	466	956	607	1387	169	349	104	1459	830	93	325	742
Ta	40·8	23·3	68·5	23·6	115	5·0	7·5	2·1	137	54·7	6·0	19·2	51·8
Li	1	4	2	1	1	27	49	12	11	n.r.	80	132	161
Zn	1009	206	638	629	1092	182	180	146	1478	300	117	276	505
Cu	38	38	5	6	4	5	17	17	11	n.r.	16	10	9
Co	1·8	2·7	2·6	2·9	2·6	3·3	1·0	0·9	5·5	n.r.	3·8	3·6	0·29
Ni	1·7	1·7	3·6	1·0	0·8	1·8	1·0	0·2	2·0	n.r.	<0·5	0·5	0·8
Sc	2·7	4·7	7·9	3·0	13	0·2	1·4	2·7	12	7	18	0·52	<0·01
Ge	1·8	2·1	1·7	2·0	0·9	1·5	1·7	0·8	0·7	n.r.	1·9	1·4	2·0
Be	21	35	18	55	37	22	28	11	16	n.r.	3·5	16	22
Mo	1·3	0·8	6·7	1·0	4·8	2·4	0·3	0·8	13	n.r.	4·4	<0·5	9
As	10	20	7·5	9·8	11	9·5	1·8	8·9	11	n.r.	3·3	2·8	11
Br	1·4	2·1	3·0	2·1	3·0	1·8	1·8	2·9	1·9	n.r.	1·5	2·9	119

P.I., peralkalinity index: molar $(Na_2O + K_2O)/Al_2O_3$. n.r., not reported; others: sum of other trace elements as oxides. Analysts: J. C. Bailey, V. Moser and the Rock Geochemistry Laboratory of the Denmark and Greenland Geological Survey.

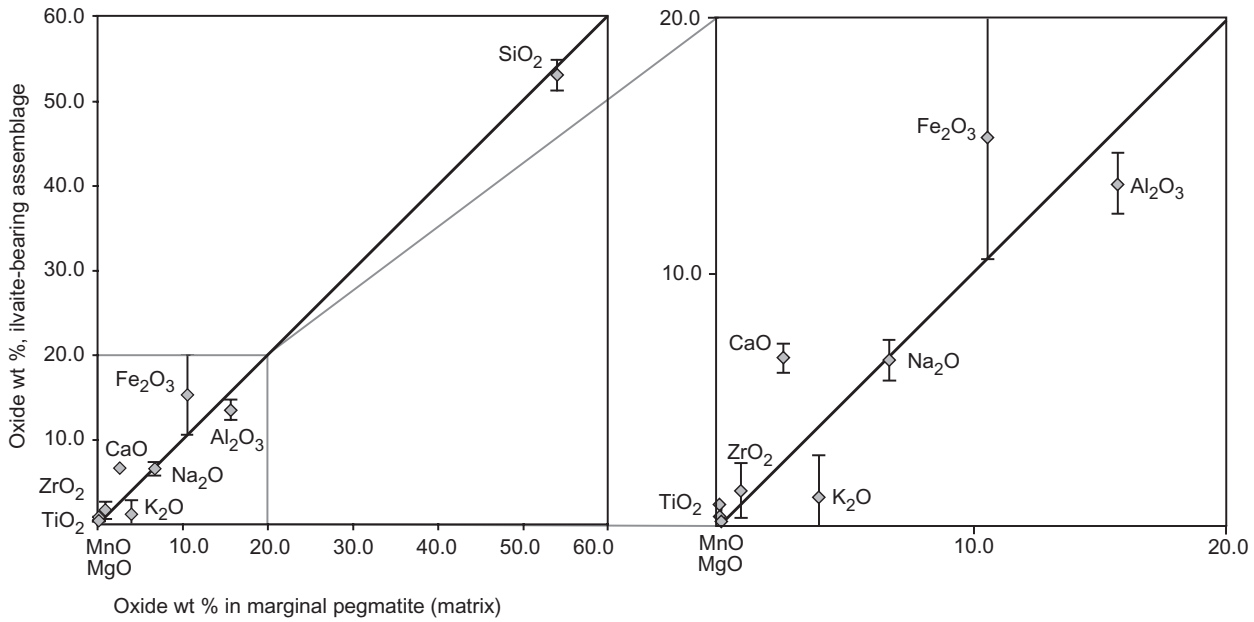

Fig. 7. Major element isocon-like plot of the average ilvaite-bearing assemblage vs the marginal pegmatite (Sørensen, 2006). Bars indicate standard deviation of the mean.

Downloaded from https://academic.oup.com/petrology/article/49/2/239/1551155 by guest on 20 April 2024

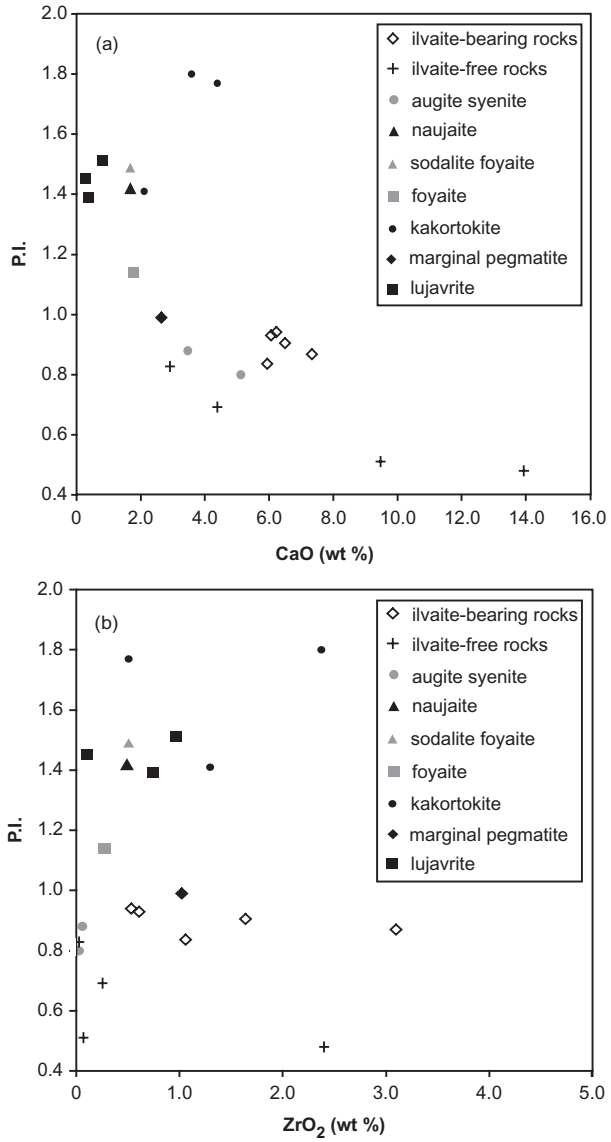

Fig. 8. CaO (a) and ZrO_2 (b) concentration vs the peralkalinity index (P.I.) of the ilvaite-bearing and -free assemblage in comparison with Ilímaussaq rocks of Sørensen (2006; marginal pegmatite) and Bailey *et al.* (2001; all other rocks).

epidote from the cavities in the Eriksfjord basalts between −1·9 and 0·5‰.

The δD values of the ilvaite-bearing whole-rock samples range from −136 to −118‰, those of the ilvaite-free assemblages from −86 to −55‰. Pure, hand-picked ilvaite varies from −148 to −136‰. Unfortunately, we could not analyse epidote because it was not possible to pick a large enough clean separate of the very fine-grained material. The Ilímaussaq augite syenites range from −94 to −88‰, the Eriksfjord basalts from −103 to −64‰, and the epidotes from the cavities have values of −44 and −35‰, respectively.

DISCUSSION

Activity calculations

The stability of the ilvaite-bearing assemblage in terms of T and fO_2 at constant P was investigated in the simplified chemical system Ca–Fe–Si–Al–O–H, considering the phases grossular (Grs), epidote (Ep), ferro-actinolite (Fac), hedenbergite (Hd), hematite (Hem) and a fluid consisting of $SiO_{2(aq)}$, H_2O and O_2. Grossular was chosen instead of andradite because another Al-bearing component was needed to balance epidote-involving reactions.

To estimate the position of relevant phase equilibria, a Schreinemakers analysis was performed for the following reactions in this system (Fig. 12):

$$Grs + Hem + SiO_2 + H_2O = Ep + Hd + O_2 \quad [Fac] \quad (1)$$

$$Hd + Hem + SiO_2 + H_2O = Fac + O_2 \quad [Grs,Ep] \quad (2)$$

$$Ep + Hd + SiO_2 + H_2O = Fac + Grs + O_2 \quad [Hem] \quad (3)$$

$$Ep + Hd = Fac + Hem + Grs + O_2 \quad [SiO_2,H_2O] \quad (4)$$

$$Hem + Grs + SiO_2 + H_2O = Ep + Fac + O_2 \quad [Hd] \quad (5)$$

$$Ep + Hd = Fac + Hem + Grs + SiO_2 + H_2O \quad [O_2]. \quad (6)$$

The rock texture shows amphibole and pyroxene to be in disequilibrium with the other phases because they are in reaction textures with ilvaite. The field in which the endoskarn mineral assemblage is stable in an fO_2 vs T diagram is thus close to or above reactions (1) and (5), where amphibole and pyroxene are not stable or become unstable in contact with epidote (Fig. 12).

Mineral end-member activities were calculated for 400°C. The activity of epidote was calculated after Bird & Helgeson (1980), that of hedenbergite after Holland (1990) and that of grossular was estimated using the program Ax of Holland & Powell (2000). The activity of $SiO_{2(aq)}$ was calculated to be temperature-dependent. The lower limit of the $SiO_{2(aq)}$ activity is given by the reaction nepheline + 2 SiO_2 = albite ($SiO_{2(aq)} = 0{\cdot}0002$ at 200°C; 0·0079 at 500°C), the upper limit defined by quartz saturation ($SiO_{2(aq)} = 0{\cdot}0027$ at 200°C, 0·0367 at 500°C). Variation of water activity results in only small changes of the position of the reactions in the fO_2–T field.

Oxygen fugacity during cooling was calculated by determining the activity-corrected log K values with Unitherm, the database program of HCh (Shvarov & Bastrakov, 1999; SUPCRT92-routine of Johnson *et al.*, 1992), for 1 and 2 kbar and variable activities of H_2O and SiO_2. The results for 1 kbar (Fig. 13) constrain the stability field of both the ilvaite-bearing and the ilvaite-free assemblages. Reaction (1) is invariably close to the hematite–magnetite (HM) buffer and spans the grey field of Fig. 13 if calculated with two different $SiO_{2(aq)}$ activities. The activity-corrected reaction (5) plots far away from geologically realistic fO_2–T conditions and beyond the conditions of Fig. 13. The occurrence of hematite in the endoskarn

Downloaded from https://academic.oup.com/petrology/article/49/2/239/1551155 by guest on 20 April 2024

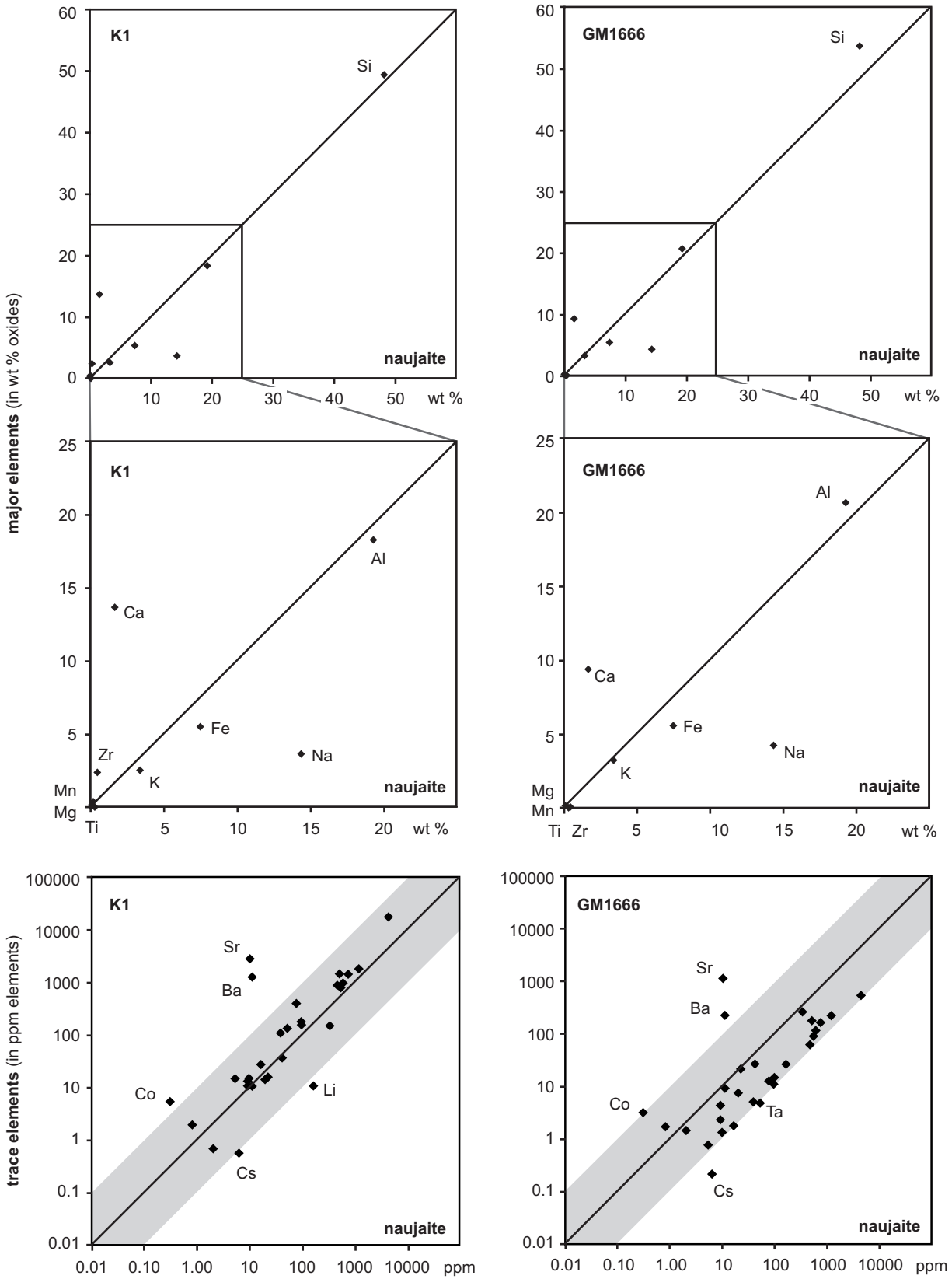

Fig. 9. Isocon-like plots of the ilvaite-free rocks vs their precursor rocks (data from Bailey *et al.*, 2001) for major and trace elements.

Downloaded from https://academic.oup.com/petrology/article/49/2/239/1551155 by guest on 20 April 2024

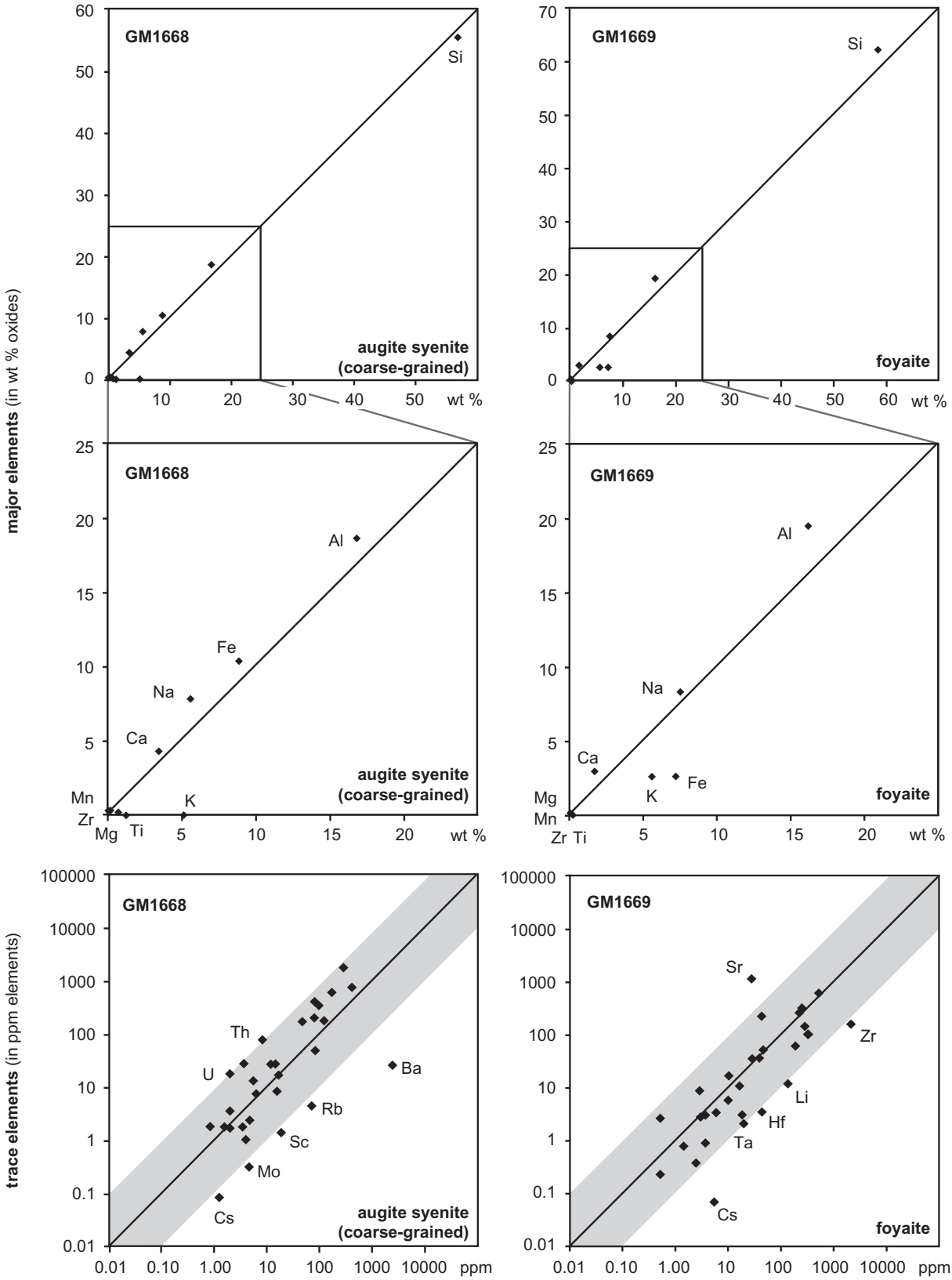

Fig. 9. Continued

Downloaded from https://academic.oup.com/petrology/article/49/2/239/1551155 by guest on 20 April 2024

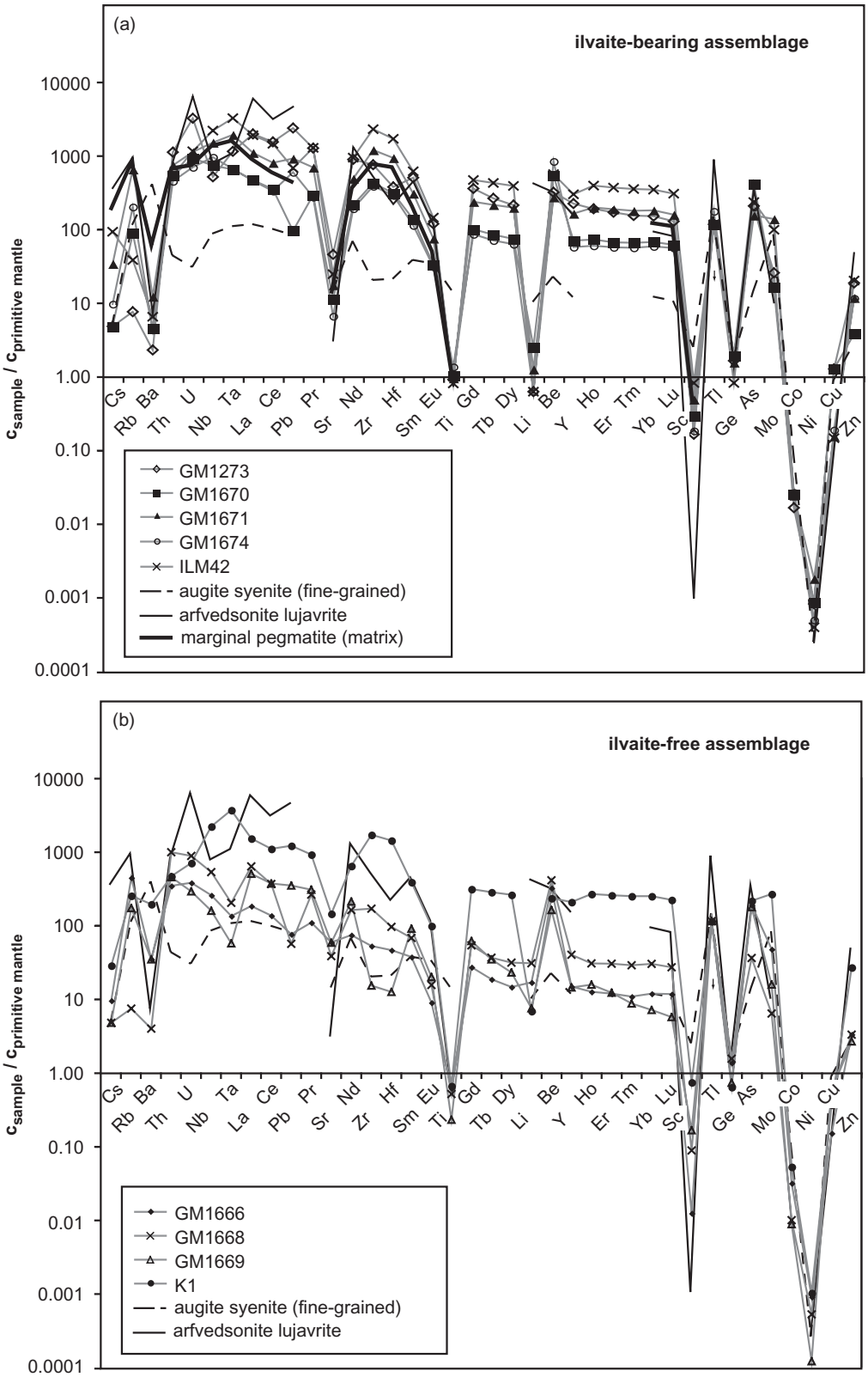

Fig. 10. Whole-rock trace element data normalized to primitive mantle values (McDonough & Sun, 1995) of the ilvaite-bearing (a) and -free (b) assemblages. Data for augite syenite and lujavrite from Bailey *et al.* (2001) give the maximum range of the trace element composition of whole-rocks in the Ilímaussaq complex; data for the matrix of the marginal pegmatite (Sørensen, 2006) are added for comparison. Unfortunately, reference data are available only for selected elements. Arrows indicate element concentrations below detection limit.

Downloaded from https://academic.oup.com/petrology/article/49/2/239/1551155 by guest on 20 April 2024

Table 5: Results of stable isotope analyses of whole-rocks and minerals of the endoskarn assemblages and some comparing whole-rocks

Sample	Sample type	Rock type	δD (‰)	$\delta^{18}O$ (‰)
ILM42	w.r.	Ilv-bearing assembl.	−130	6·2
GM1273	w.r.	Ilv-bearing assembl.	−118	4·7
GM1670	w.r.	Ilv-bearing assembl.	−131	3·5
GM1671	w.r.	Ilv-bearing assembl.	−123	4·7
GM1674	w.r.	Ilv-bearing assembl.	−136	3·0
GM1670	Ilv	Ilv-bearing assembl.	−136	−4·7
GM1674	Ilv	Ilv-bearing assembl.	−145	−3·6
ILM40	Ilv	Ilv-bearing assembl.	−148	−4·0
ILM40	Ep	Ilv-bearing assembl.	—	−1·1
ILM40	Grt	Ilv-bearing assembl.	—	−1·8
GM1670	Grt	Ilv-bearing assembl.	—	−3·3
ILM40	Fsp	Ilv-bearing assembl.	—	7·2
GM1670	Fsp	Ilv-bearing assembl.	—	5·9
GM1674	Fsp	Ilv-bearing assembl.	—	7·2
K1	w.r.	Ilv-free assembl.	−74	4·8
GM1666	w.r.	Ilv-free assembl.	−55	4·5
GM1668	w.r.	Ilv-free assembl.	−86	4·9
GM1669	w.r.	Ilv-free assembl.	−67	6·8
GM1330	w.r.	augite syenite	−94	6·7
GM1857	w.r.	augite syenite	−88	6·4
EF024	w.r.	EF-basalts	−103	4·3
EF072	w.r.	EF-basalts	−92	5·5
EF075	w.r.	EF-basalts, much Ep	−65	1·9
EF087	w.r.	EF-basalts, slightly ep	−84	−0·1
EF140	w.r.	EF-basalts, slightly ep	−94	1·8
EF141	w.r.	EF-basalts, slightly ep	−93	−0·8
EF144	w.r.	EF-basalts, completely ep	−64	−1·8
EF168	w.r.	EF-basalts	−73	3·8
B72	Ep	Ep–Qtz cavity in EF-bas.	−35	0·5
B73	Ep	Ep–Qtz cavity in EF-bas.	−44	−1·9

w.r., whole-rock; EF, Eriksfjord; ep, epidotized.

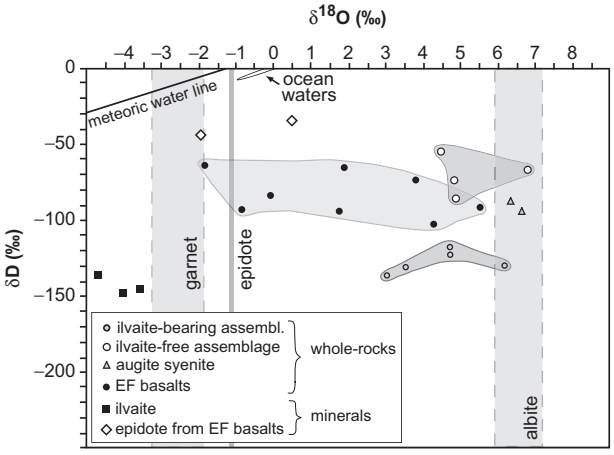

Fig. 11. $\delta^{18}O$ and δD values of whole-rock samples and minerals. Albite, garnet and epidote from the ilvaite-bearing assemblage are shown as bars because of the lack of hydrogen isotope data. For comparison, other Ilímaussaq and Eriksfjord (EF) samples are plotted.

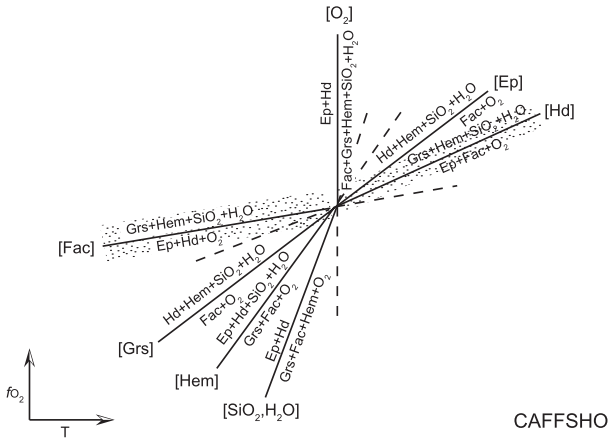

Fig. 12. Schreinemakers analysis of the Al_2O_3–CaO–FeO–Fe_2O_3–SiO_2–H_2O system including the phases grossular (Grs), epidote (Ep), ferro-actinolite (Fac), hedenbergite (Hd), hematite (Hem), and a fluid consisting of $SiO_{2(aq)}$, H_2O and O_2.

assemblage restricts the field to the hematite-stable side of the buffer curve and, hence, to the range of FMQ + 5 to FMQ + 7.

Gustafson (1974) performed ilvaite stability experiments at 2 kbar. Because the position of the calculated reaction curves and invariant points of our study does not change significantly between 1 and 2 kbar, we regard the ilvaite reaction of Gustafson (1974) to be at least a temperature approximation for our assemblages (Fig. 13). However, it is important to note that Gustafson's experiments were performed in the pure C–F–S–O–H system, whereas the ilvaites of our study contain up to 4·2 wt % MnO, which may change the precise location of the reaction curve in T–fO_2 space. In accordance with the isotope fractionation temperatures detailed below, we conclude that the uncertainty of the curve in Fig. 13 is about 50–100°C, implying that (based on Fig. 13) the main endoskarn formation probably occurred between 400 and 500°C. However, phase relations after Liou *et al.* (1983), plotted in Fig. 13, indicate that prehnite in the ilvaite-free assemblage formed between 300 and 340°C and at log fO_2 values between −26 and −29. In accordance with petrographic observations (see above), we conclude that prehnite did not grow during the main-stage endoskarn formation, but later at lower temperatures.

It is interesting to note that our temperature results for the formation of prehnite in the ilvaite-free assemblage

Downloaded from https://academic.oup.com/petrology/article/49/2/239/1551155 by guest on 20 April 2024

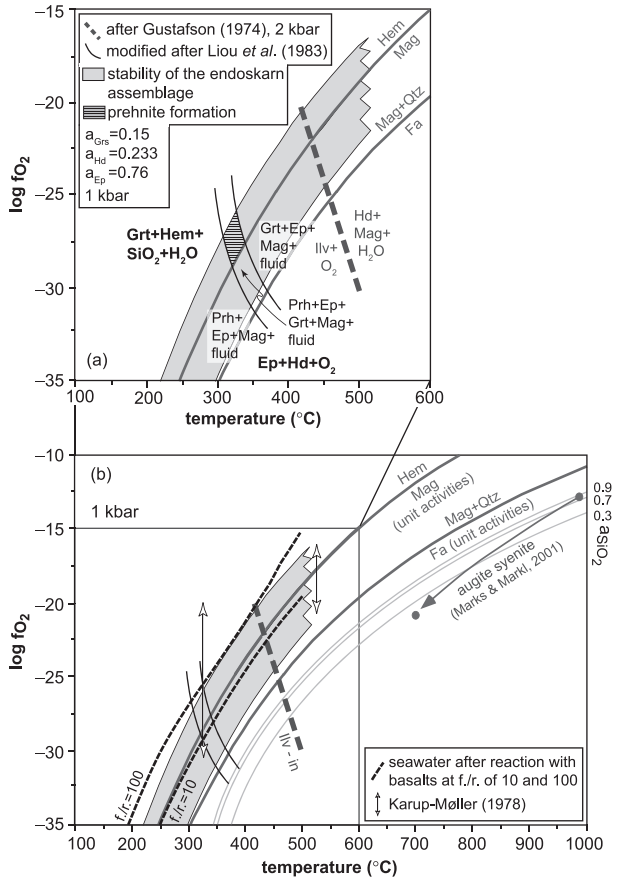

Fig. 13. (a) Stability constraints for the endoskarn assemblages in a log fO_2–T diagram. Unit activities were used unless specified otherwise. Stability constraints of Gustafson (1974) and Liou *et al.* (1983) were added for ilvaite- and prehnite-bearing assemblages, respectively. The ilvaite-stability curve after Gustafson (1974) is plotted as a dashed line, to illustrate an uncertainty, as it is for the pure system, whereas the ilvaites of our studies contain additional Mn. (See text for discussion.) (b) Stability constraint for the endoskarn assemblages in comparison with the fO_2–T evolution during fractionation of Ilímaussaq melts, after Marks & Markl (2001). The bold dashed lines for different f./r. (fluid/rock) ratio constrain seawater composition after spilitization reactions with the basalts (see text for details). Mineral name abbreviations after Kretz (1983), except ilvaite (Ilv).

agree well with T–fO_2 data derived from hydrothermal sulphide assemblages in Ilímaussaq late-stage veins determined by Karup-Møller (1978, Fig. 13).

In summary, phase relations indicate that the Ca-rich assemblages formed at temperatures below 500°C at $SiO_{2(aq)}$ activities between 0·001 and 0·02, and at fO_2 values slightly above HM (between FMQ+5 and FMQ+7). The formation of ilvaite in the endoskarns is limited to Fe-rich precursor whole-rock compositions.

Whole-rock constraints

Based on field observations, textures and whole-rock compositions, the endoskarn assemblages are not related to carbonate rocks. Furthermore, textures and the similarity between the primitive mantle-normalized trace element patterns (after McDonough & Sun, 1995) of the endoskarns of this study and the range of Ilímaussaq rocks (Bailey *et al.*, 2001; Sørensen, 2006; Fig. 10) suggest that rocks from the peralkaline complex itself were transformed into the endoskarns. To understand the mass transport of elements related to the formation of the endoskarn assemblages in the Ilímaussaq complex, isocon-like diagrams (Figs 7 and 9) were used. The inferred precursor rock for the ilvaite-bearing assemblages, the marginal pegmatite, is heterogeneous with respect to grain size and mineralogical composition: it comprises pegmatitic Fe-richer parts with large amphibole crystals and a fine-grained matrix that is poorer in Fe but with an enrichment in eudialyte and, hence, in Ca and Zr. Accordingly, these elements are also highly variable in the endoskarn assemblages (Figs 7 and 9). The only persistent feature in all of the samples is that the Ca content of the ilvaite-bearing assemblage is fairly constant and significantly higher than in the unaltered matrix of the marginal pegmatite (Table 4). This matrix is used as the best approximation to the composition of the unaltered pegmatitic part, as there are no whole-rock data for the pegmatitic veins available at present. The matrix generally contains less arfvedsonite than the pegmatitic part and, hence, the ilvaite-bearing endoskarn assemblage is consistently richer in Fe than the unaltered matrix (Fig. 7). On the other hand, the matrix commonly contains more eudialyte than the pegmatitic veins, and thus it should have higher amounts of Ca. The fact that the opposite is true points to an enrichment of Ca in the studied rocks (Fig. 7).

Two of the four whole-rock samples of the ilvaite-free assemblage (GM1668 and GM1669) fit fairly well with the representative analyses of the coarse-grained augite syenite and the foyaite, respectively (Fig. 9). Both have CaO <5 wt %, but slightly more than their presumed precursors. The two samples with clear naujaite texture (GM1666 and K1) fit well with the representative naujaite of Bailey *et al.* (2001), except for a strong enrichment in Ca and a depletion in Na. It is evident that the presence of the very Fe-rich amphiboles or the generally much higher Fe content of the amphibole-bearing pegmatitic parts was a necessary prerequisite for the formation of ilvaite. The Fe-richer whole-rock composition is also reflected in the mineral compositions (e.g. of the garnets or the epidotes–allanites).

The source of the calcium

There are two ways to explain the gain of Ca: from internal or from external sources. We explore both possibilities. Internal sources of Ca in the intrusion from which Ca could be redistributed and enriched in the endoskarn assemblages could be clinopyroxene, feldspar and eudialyte. These minerals contain up to about 21, 4, and 10 wt % CaO, respectively (clinopyroxene, Marks & Markl, 2001;

Downloaded from https://academic.oup.com/petrology/article/49/2/239/1551155 by guest on 20 April 2024

feldspar, Larsen, 1981; eudialyte, Johnsen & Gault, 1997) and late-magmatic metasomatic reactions involving Na-rich peralkaline fluids could release Ca according to the following reactions:

$$\text{feldspar}: CaAl_2Si_2O_8 + 2Na^+ + 4SiO_2 = 2NaAlSi_3O_8 + Ca^{2+}$$

$$\text{clinopyroxene}: 2CaFeSi_2O_6 + 2Na^+ + 2H^+ + 0{\cdot}5O_2 = 2NaFeSi_2O_6 + 2Ca^{2+} + H_2O$$

$$\text{eudialyte (schematic)}: \text{eudialyte} + \text{fluid} = \text{allanite} + \text{zircon} + \text{albite}.$$

In this model, the Ca from feldspar and clinopyroxene would have been released into the fluid for redistribution and fixation in new minerals, leaving behind pure albite and aegirine. Additionally, eudialyte, a major REE- and Zr-rich mineral of the agpaitic rocks in Ilímaussaq (Sørensen, 1992), was transformed, releasing Ca, Zr and REE, which were incorporated into the zircon and the allanite present in the samples.

In principle, this would be a viable process, and extensive late-magmatic fluid–rock interaction is recorded in many Ilímaussaq rocks (see e.g. Schönenberger, 2006). However, it is unclear to us why Ca from large areas in the intrusion should be enriched at the point of endoskarn formation. Such a scenario would be necessary, as there is no way to generate the Ca enrichment on a volume-conservative basis, and thus the underlying process would remain enigmatic. Therefore, we prefer the second explanation of Ca enrichment, which involves an external source (i.e. a Ca-rich external fluid). In this case, it would be possible to derive Ca from the metasomatic alteration of the overlying Eriksfjord basalts, which display ample evidence for alteration in the greenschist facies (epidote–chlorite–quartz assemblage).

Metasomatic phenomena in and around peralkaline rocks: a comparison

Phase assemblages formed by metasomatic alteration and involving external fluids are well known from alkaline complexes (e.g. Sindern & Kramm, 2002; Savatenkov *et al.*, 2004). Salvi & Williams-Jones (1990, 1996, 2006) and Boily & Williams-Jones (1994) studied the role of hydrothermal processes in the peralkaline Strange Lake complex, Canada. Salvi *et al.* (2000) investigated the agpaitic rocks of the Tamazeght complex, Morocco, with respect to HFSE mobilization in, and deposition from, F- and Ca-bearing fluids. In this case, HFSE were transported as fluoride complexes in a F-rich orthomagmatic fluid and deposited by mixing with a Ca-enriched, externally derived meteoric fluid (Salvi & Williams-Jones, 1996). Khadem Allah *et al.* (1998) described Ca enrichment in nepheline syenites of the Tamazeght Complex in contact with carbonate country rocks, which is recorded by the occurrence of, for example, pectolite and cancrinite and by an enrichment in the diopside component of clinopyroxenes. Fluid-related alteration phenomena are also known from around the Gardar intrusions in South Greenland. Fenitization is known from the volcanic rocks overlying the lujavrites in the northern part of the Ilímaussaq intrusion (Sørensen *et al.*, 1974; Kunzendorf *et al.* 1982; Sørensen & Larsen, 2001). Pitchblende occurs in fractures in the basement granite (Armour-Brown *et al.*, 1983). The fracture zones are fenitized and contain perthitic feldspar and interstitial chlorite, iron oxides, carbonates, and as common accessories apatite, fluorite and zircon. Ranløv & Dymek (1991) delineated aegirine-rich zones of metasomatic alteration on the Narssaq Peninsula in the northeastern part of the Ilímaussaq intrusion. Hansen (1968) described in the same area fractures filled with quartz, albite, microcline, aegirine, calcite and hematite, with accessories such as allanite and apatite, and fenitized rocks between the fractures. The mineralizations were related to low-temperature fluids derived from the intrusive complexes of Ilímaussaq and Igaliko. Wegmann (1938), who found abundant fluorite in the country rock of the intrusion around Tunulliarfik, concluded that F mobilization affected the entire area.

Fluid-related alteration is also found within Gardar plutons; for example, in andradite-bearing autometasomatic assemblages described by Marks *et al.* (2003) from the peralkaline Puklen pluton. Parsons *et al.* (1991), Finch (1995), Rae *et al.* (1996) and Coulson (1997, 2003) described metasomatic alteration phenomena, which involved both late-magmatic and external fluids within other Gardar complexes. Fluid-involving alterations in the Ilímaussaq complex were mentioned by Ussing (1912), who described a broad (≤100 m), red, ferric oxide- and fluorite-rich band of alteration in the northern part of the intrusion. Except for feldspar, the mineral assemblages of naujaite and lujavrite are replaced by hematite, fluorite, natrolite, chlorite and zeolites at this locality. Other regions within the Ilímaussaq intrusion where pneumatolytic alteration took place are shown on the maps of Ferguson (1964) and Bohse *et al.* (1971).

In summary, metasomatic processes involving Ca-enriched fluids are well known from peralkaline complexes in general, and from the Gardar Province in particular. We believe that the Ilímaussaq endoskarns are just a particularly spectacular and unusual example of such phenomena. We will now proceed to characterize the source and chemical evolution of the external metasomatizing fluid.

Isotopic constraints

The large range in whole-rock $\delta^{18}O$ for the ilvaite-bearing assemblage (Fig. 11) may be caused by modal variations of ilvaite ($\delta^{18}O = -4{\cdot}7$ to $-3{\cdot}6$‰), garnet ($\delta^{18}O = -1{\cdot}8$ and $-3{\cdot}3$‰), epidote ($\delta^{18}O = -1{\cdot}1$‰) and albite ($\delta^{18}O = 5{\cdot}9$–$7{\cdot}2$‰). The mineral data reveal a large

Downloaded from https://academic.oup.com/petrology/article/49/2/239/1551155 by guest on 20 April 2024

isotopic fractionation between albite and the other minerals and a smaller one between ilvaite and garnet, ilvaite and epidote, and garnet and epidote.

To derive temperature information, we studied mineral–mineral isotopic equilibria by using the mineral–H_2O fractionation coefficients of Zheng (1993*a*, 1993*b*). Because it is well known that some of Zheng's data do not reproduce experimental fractionation factors, we applied various sets of mineral–H_2O fractionation factors to our data and compared the respective results. Experimentally determined fractionation factors exist for albite–H_2O (Friedman & O'Neil, 1977; Matsuhisa *et al*., 1979) and for andradite–H_2O (Taylor, 1976; Kieffer, 1982), but not for ilvaite–H_2O and epidote–H_2O. Experimentally derived factors, however, are ascertained for distinct ranges of temperature only, and our inferred conditions do not always fall into these ranges. Our calculations therefore provide only an estimate of the temperature range in which the alteration processes took place.

Most of the equilibria not involving albite indicate that the ilvaite-bearing endoskarn assemblage formed in the range 400–600°C (Table 6). This range slightly exceeds the upper temperature limit of ilvaite stability according to Gustafson (1974), which most probably is the result of additional elements present in our assemblage and not present in Gustafson's experiments (e.g. Mn).

Calculation of epidote–albite equilibria showed that, regardless of the fractionation coefficients used, these two minerals are not in isotopic equilibrium. Most other equilibria involving albite invariably indicate temperatures below 285°C, regardless of the coefficients used (Table 6). We interpret this result to indicate isotopic re-equilibration of albite at low temperatures. As feldspars are known to re-equilibrate to very low T (Giletti *et al*., 1978), it is highly likely that the other three minerals record the fluid during formation of the assemblages, whereas the feldspar probably records re-equilibration with (potentially the same) fluid during cooling.

In summary, textural observations, phase relations and oxygen isotope temperatures clearly indicate that the endoskarn assemblages were modified twice after their formation: at 300–350°C prehnite formed in the ilvaite-free assemblage (see also Fig. 13), and below ~250°C albite re-equilibrated with a cooled fluid. In both these cases, we cannot determine whether the same, but cooled fluid or a new fluid influx was responsible for the alteration.

We suggested above that an external fluid was probably responsible for the Ca enrichment and the endoskarn mineralization. An approximation to the $\delta^{18}O$ signature of this fluid in isotopic equilibrium with the analysed minerals was calculated using the fractionation coefficients between mineral and H_2O of Zheng (1993*a*, 1993*b*) (Fig. 14). The oxygen isotopic composition of the fluid calculated for each mineral as a function of temperature show an intersection for epidote, ilvaite and garnet at a minimum temperature of ~450°C and a $\delta^{18}O$ value of about 0‰ (Fig. 14)–close to modern seawater–whereas albite is not in isotopic equilibrium at this temperature (see above).

The hydrogen isotope signature of the ilvaite-bearing assemblage ($\delta D = -136$ to -118‰) is dominated by ilvaite ($\delta D = -148$ to -136‰) as the dominant hydrogen-bearing mineral. The values for the ilvaite-free assemblages are accordingly higher ($\delta D = -86$ to -55‰), within the typical range of magmatic rocks and fluids (Sheppard, 1986; Taylor & Sheppard, 1986). Unfortunately, the H isotopic composition of epidote

Table 6: Mineral-mineral equilibrium temperatures calculated via mineral-H_2O fractionation factors from different sources

Mineral pairs excluding albite; reference of fractionation factor min–H_2O	Calculated range of equilibrium (°C)
Ilvaite–andradite	
Ilvaite: Zheng (1993*a*), andradite: Taylor (1976)	350–490
Ilvaite: Zheng (1993*a*), andradite: Kieffer (1982)	490–610
Ilvaite and andradite: Zheng (1993*a*, 1993*b*)	380–600
Epidote–andradite	
Epidote: Zheng (1993*a*), andradite: Taylor (1976)	500
Epidote and andradite: Zheng (1993*a*, 1993*b*)	400
Epidote–ilvaite	
Epidote and ilvaite: Zheng (1993*a*)	500–720
Mineral pairs including albite	
Andradite–albite	
Andradite: Taylor (1976), albite: Matsuhisa *et al*. (1979)	no result
Andradite: Taylor (1976), albite: Friedman & O'Neil (1977)	300–307
Andradite: Kieffer (1982), albite: Matsuhisa *et al*. (1979)	no result
Andradite: Kieffer (1982), albite: Friedmann & O'Neil (1977)	206–212
Andratite and albite: Zheng (1993*b*)	160–166
Ilvaite–albite	
Ilvaite: Zheng (1993*a*), albite: Matsuhisa *et al*. (1979)	210–237
Ilvaite: Zheng (1993a), albite: Friedman & O'Neil (1977)	220–285
Ilvaite and albite: Zheng (1993*a*, 1993*b*)	212–233
Epidote–albite	
All possible combinations	no result

Downloaded from https://academic.oup.com/petrology/article/49/2/239/1551155 by guest on 20 April 2024

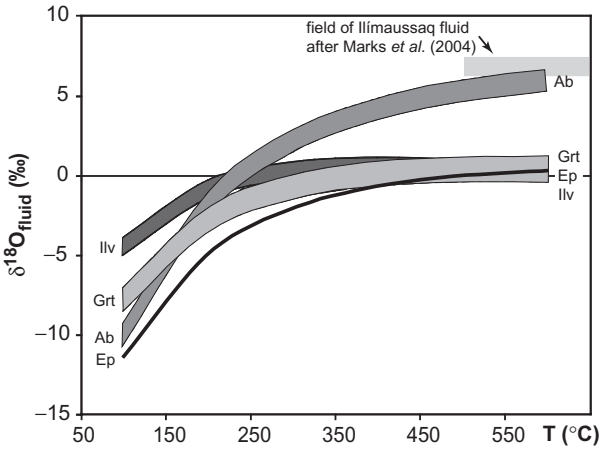

Fig. 14. $\delta^{18}O$ composition of the fluid in equilibrium with the analysed minerals at temperatures between 50 and 600°C calculated using the fractionation coefficients of Zheng (1993*a*, 1993*b*). The fluid compositions plot in fields rather than on lines because of the variations in the mineral chemistry. Grey, frameless bar indicates fluids corresponding to the Ilímaussaq amphiboles studied by Marks *et al.* (2004) that were calculated for temperatures between 500 and 800°C.

from the endoskarn assemblages could not be analysed because of lack of enough pure sample material. Based on the temperature-independent fractionation coefficient of Qian & Guo (1993) for 350–550°C, the δD signature of the fluid in isotopic equilibrium with ilvaite is estimated to lie between −54 and −40‰. Thus, the fluid shows a trend towards isotopically heavier compositions. The temperature independence of the coefficient and the uncertainties in hydrogen isotope fractionation coefficients in general may be the reasons for the calculated fluid not plotting on the modern meteoric water trend in Fig. 11. The δD signature of the fluid in isotopic equilibrium with the epidotes from the Eriksfjord basalts (δD = −35 and −44‰), however, is +6 and −3‰, respectively, for 400°C, and 10 and 1·4‰ for 500°C [calculated with the fractionation coefficients of Chacko *et al*. (1999)], which is reasonably close to modern seawater.

We admit that we do not know if the stable isotope composition of modern seawater is similar to the seawater isotope composition at 1·16 Ga, but in the absence of any evidence to the contrary, and given the geological evidence for the presence of pillow-basalts in the Eriksfjord Formation, we consider it reasonable to assume the involvement of seawater.

In summary, it appears that seawater circulating through the Eriksfjord basalts was one of the driving forces of metasomatism responsible for the formation of the endoskarns at Ilímaussaq. The structures along which seawater was circulating in the ground are arranged erratically and thus there is no uniform alteration. The pillow structures in the Eriksfjord basalts (Emeleus & Upton, 1976) and the ubiquitous occurrence of chlorite–epidote–quartz assemblages in the basalts are evidence of both a temporarily marine environment and spilitization reactions, and hence of the necessary prerequisites of our model. Furthermore, the D and O isotopic compositions of the epidotes from basalts analysed in the course of this study agree with equilibration with a fluid close to (modern) seawater composition.

To constrain the seawater alteration process quantitatively, we calculated fluid–rock equilibria for a fluid of typical (modern) seawater composition during progressive fluid–rock interaction between 50°C and 300 bar, and 500°C and 1000 bar in the system Si–Al–Fe–Mg–Ca–Na–K–C–S–Cl–O–H. Calculations were carried out in different runs with effective fluid/rock ratios of 0·1, 1, 10 and 100 and along the constructed geotherm $P = 100 + 4{\cdot}25\,T - 0{\cdot}005\,T^2$. It is noted that the term effective fluid/rock ratio is used here for the time-integrated fluid flux the rock has experienced. The primary seawater composition is from Millero (2004), recalculated to the system Mg–Ca–Na–K–C–S–Cl–O–H with its dissolved oxygen content constrained by equilibrium with O_2 gas at (modern) atmospheric partial pressure. The composition of a typical Eriksfjord basalt was taken from Halama *et al.* (2003, sample EF 059).

Calculations were performed with the HCh software package (Shvarov & Bastrakov, 1999), which models heterogeneous equilibria and reaction progress by minimization of the Gibbs' free energy of the total system (Shvarov, 1978, 1981). The thermodynamic data for aqueous species are from the SUPCRT92 database and subsequent updates (Johnson *et al.*, 1992; Shock *et al.*, 1997; Sverjensky *et al.*, 1997). Data for silicate, oxide, hydroxide and carbonate minerals were taken from the internally consistent dataset of Holland & Powell (1998). An extended Debye–Hückel model using the b-gamma equation for NaCl as background electrolyte was applied for calculations of activity coefficients of aqueous species (Oelkers & Helgeson, 1990; Shock *et al.*, 1992).

The results of our calculations indicate that the fluids had equilibrium Ca concentrations of $6{\cdot}0 \times 10^{-3}$ and $5{\cdot}2 \times 10^{-3}$ mol/kg Ca at fluid/rock ratios of 10 and 100, respectively, for 400°C, and of $1{\cdot}1 \times 10^{-2}$ and $3{\cdot}6 \times 10^{-3}$ for 500°C (Table 7, Fig. 15). Hence, reasonable amounts of about 10^{11} kg fluid (corresponding to a rock volume of about 0·001 km^3) would be sufficient to explain the Ca enrichment of the endoskarns, even if all Ca would have to be added. The oxygen fugacity of these fluids in equilibrium with the altered basalt is around HM and HM + 4 for fluid/rock ratios of 10 and 100, respectively.

The high fluid/rock ratio would also explain why the O isotopic signature of the fluid remained essentially unchanged during the spilitization reactions. The analysed basalt samples, in contrast, show much lighter values

Downloaded from https://academic.oup.com/petrology/article/49/2/239/1551155 by guest on 20 April 2024

Table 7: Compositon of seawater in equilibrium with the Eriksfjord basalt along a constructed geotherm (see text for details)

T(°C)	500	450	400	300	200
P (bar)	1005	996	970	865	690
Fluid/rock = 10					
Al (mol/kg)	1·13E−02	1·64E−02	6·00E−03	6·50E−03	7·69E−03
Fe (mol/kg)	3·35E−03	5·83E−04	2·26E−05	2·21E−07	2·21E−08
Mg (mol/kg)	7·99E−04	2·81E−04	3·20E−05	7·78E−06	1·46E−06
Ca (mol/kg)	1·13E−02	1·64E−02	6·00E−03	6·50E−03	7·69E−03
Na (mol/kg)	5·27E−01	5·24E−01	5·49E−01	5·52E−01	5·74E−01
K (mol/kg)	1·61E−02	1·61E−02	1·61E−02	1·61E−02	1·62E−02
log fO_2	−19·56	−21·90	−24·57	−31·04	−39·85
pH	5·35	5·27	5·55	5·80	6·70
Fluid/rock = 100					
Al (mol/kg)	1·34E−05	3·56E−06	1·82E−06	6·19E−07	1·22E−07
Fe (mol/kg)	9·43E−03	8·07E−03	4·97E−03	3·98E−04	1·57E−04
Mg (mol/kg)	1·81E−02	2·04E−02	2·41E−02	3·03E−02	3·24E−02
Ca (mol/kg)	3·57E−03	4·59E−03	5·19E−03	5·48E−03	9·88E−03
Na (mol/kg)	5·01E−01	5·01E−01	5·01E−01	5·01E−01	5·01E−01
K (mol/kg)	1·08E−02	1·08E−02	1·08E−02	1·08E−02	1·08E−02
log fO_2	−15·11	−18·14	−21·29	−27·04	−34·71
pH	4·57	4·22	3·98	3·84	4·30

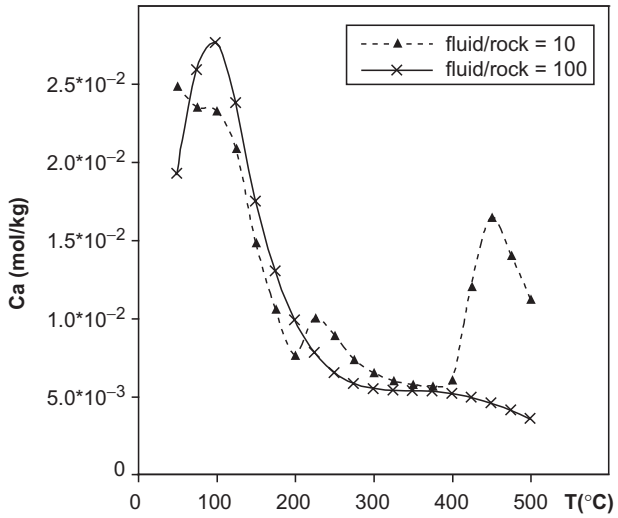

Fig. 15. Variability of the Ca content (mol/kg) of a seawater fluid passing through the Eriksfjord basalts along a constructed geotherm (see text for details). The shape of the curves is a result of variable fluid–fluid and fluid–rock equilibria.

(Fig. 11) than typical basalts, which are expected to have values around 5–7‰ (Taylor & Sheppard, 1986). The spread in $\delta^{18}O$ values in Fig. 11 hence probably records the intensity of the spilitization process.

We calculated the change in the isotope signature of water using the formula of Taylor (1977):

$$\frac{W}{R} = \frac{\delta^{f}_{Rock} - \delta^{i}_{Rock}}{\delta^{i}_{Rock} - (\delta^{f}_{Rock} - \Delta)}$$

where W and R are the relative atomic per cent of water and rock oxygen, respectively, in the bulk system, δ^{i} and δ^{f} the initial and final isotope values, respectively, and Δ is $(\delta^{f}_{Rock} - \delta^{f}_{H_2O})$. The fresh Eriksfjord basalts have a $\delta^{18}O$ value between 5 and 6‰ (Halama *et al*., 2003), whereas the most altered sample has a $\delta^{18}O$ value of −1·8‰ (EF 144, this study). The calculations after Taylor (1977) reveal that the fluid's isotope composition stays close to 0‰ for fluid/rock ratios of 10 (0·4‰) and 100 (0·04‰). Lower ratios result in much higher $\delta^{18}O$ values of the fluid. By analogy, the results for H isotopes are close to 0‰ for fluid/rock ratios of 10 (−0·1‰) and 100 (−0·01‰), when taking EF072 as the fresh basalt sample ($\delta D = -92‰$) and EF 144 as the most altered one ($\delta D = -64‰$).

SUMMARY AND CONCLUSIONS

This study investigated parts of the western marginal portion of the peralkaline Ilímaussaq intrusion, where

Downloaded from https://academic.oup.com/petrology/article/49/2/239/1551155 by guest on 20 April 2024

persodic igneous rocks were altered to Ca-rich endoskarn assemblages with epidote–allanite, hydrogarnet, and ilvaite or prehnite. These endoskarns are significantly enriched in Ca in comparison with their precursor rocks, which were inferred on the basis of whole-rock compositions and textures. The very heterogeneous nepheline syenitic marginal pegmatite is the precursor for the ilvaite-bearing assemblages, whereas various other Ilímaussaq syenites (e.g. naujaite, augite syenite, foyaite) are the precursors of the ilvaite-free assemblages. The occurrence of ilvaite appears to depend on the presence of large amounts of Fe-rich amphibole in the precursor rock. Stable isotope investigations yielded temperatures of about 500°C, and activity-corrected thermodynamic calculations revealed oxygen fugacities between FMQ + 5 and FMQ + 7 (slightly above the HM buffer) as conditions of formation for the endoskarn assemblage. Textures and phase relations indicate prehnite to have formed at about 300–340°C during cooling of the complex and after the formation of the endoskarns. Stable isotope data for albite suggest re-equilibration at even lower temperatures.

In the absence of any carbonate rocks in the vicinity of Ilímaussaq, there remain two different possible sources of Ca: redistribution of Ca released during late- to post-magmatic breakdown of Ca-bearing magmatic phases or externally derived Ca-rich fluids, which entered the complex along faults and along the margins of the complex. Based on geological evidence, we prefer the second possibility. Stable isotope compositions of minerals from the endoskarn assemblage indicate that the fluid had the $\delta^{18}O$ signature of modern seawater, which is consistent with the presence of pillow structures in the basalts of the Eriksfjord Formation. These basalts are assumed to be only slightly older than the intrusion (Paslick *et al.*, 1993), which makes the presence of seawater at the time of intrusion plausible. Therefore, field observations and isotopic data are best explained by postulating the influx of seawater into the Ilímaussaq intrusion and, hence, we prefer an external Ca-rich fluid as the major Ca source for our endoskarn assemblage. However, we cannot rule out completely the possibility that some of the Ca enrichment is related to internal redistribution within the intrusion during late-magmatic autometasomatic alteration processes.

Fluid–rock interaction ('spilitization') between seawater and the Eriksjord basalts at temperatures between 10 and 500°C enriched the fluid in Ca, necessary for the formation of the endoskarn assemblages. High fluid/rock ratios of 10–100 would explain both the basically unchanged $\delta^{18}O$ signature of the fluid and the highly oxidized nature of the fluid above the HM buffer. Reasonable amounts of about 10^{11} kg fluid (a rock volume of about 100 m × 100 m × 100 m) with Ca contents of around 10^{-3} mol/kg Ca are sufficient to explain the Ca enrichment in the endoskarns of, for example, the marginal pegmatite.

Earlier studies (Marks & Markl, 2001; Markl *et al.*, 2001; Marks *et al.* 2004) suggested a closed system for the evolution of the Ilímaussaq intrusion. Although we now have presented evidence for the infiltration of external fluids, it is important to note that this happened after differentiation and solidification of the pluton. Accordingly, magmatic crystallization proceeded in a closed system, which, however, experienced external metasomatism along its margins and along faults during late-magmatic cooling, while it was still at temperatures of about 300–500°C.

ACKNOWLEDGEMENTS

We would like to thank Thomas Wagner for sharing his results on the thermodynamic modelling, Thomas Wenzel for his help with the microprobe, Gabi Stoschek and Bernd Steinhilber for the stable isotope analyses, and Regina Freiberger for her hints regarding hydrogarnets. We are grateful to John C. Bailey, Vagn Moser, and the Rock Geochemistry Laboratory of the Denmark and Greenland Geological Survey for performing the whole-rock analyses. Henning Sørensen is thanked for his information about and his photograph of the marginal pegmatite. Together with Anton Chakhmouradian, Axel Liebscher and editor Reto Gieré, he provided a very insightful review, which helped to improve the quality of this work significantly, as did comments by Michael Marks on an earlier version of this manuscript. All their input is gratefully acknowledged. The research for this publication was supported by the Alfried Krupp Prize for Young University Teachers of the Krupp Foundation. This paper is *Contribution to the Mineralogy of Ilímaussaq* No. 129.

REFERENCES

Andersen, S., Bohsen, H. & Steenfelt, A. (1988). *Geological map of Greenland 1:20 000, the southern part of the Ilímaussaq complex, South Greenland*. Denmark: Grønlands Geologiske Undersøgelse–Geodætisk Institut.

Armour-Brown, A., Steenfelt, A. & Kunzendorf, H. (1983). Uranium districts defined by reconnaissance geochemistry in south Greenland. *Journal of Geochemical Exploration* **19**, 127–145.

Armstrong, J. T. (1991). Quantitative element analysis of individual microparticles with electron beam instruments. In: Heinrich, K. F. J. & Newbury, D. E. (eds) *Electron Probe Quantitation*. New York: Plenum, pp. 261–315.

Bailey, J. C., Gwozdz, R., Rose-Hansen, J. & Sørensen, H. (2001). Geochemical overview of the Ilímaussaq alkaline complex, South Greenland. In: Sørensen, H. (ed.) *The Ilímaussaq Alkaline complex, South Greenland: status of mineralogical research with new results. Geology of Greenland Survey Bulletin* **190**, 35–53.

Bailey, J. C., Sørensen, H., Andersen, T., Kograko, L. N. & Rose-Hansen, J. (2006). On the origin of microrhythmic layering in arfvedsonite lujavrite from the Ilímaussaq alkaline complex, South Greenland. *Lithos* **91**, 301–318.

Bartholomé, P. & Dimanche, F. (1967). On the paragenesis of ilvaite in Italian skarns. *Annales de la Société Géologique de Belgique* **90**, 533–558.

Bird, D. K. & Helgeson, A. C. (1980). Chemical interaction of aqueous solutions with epidote–feldspar mineral assemblages in geologic systems. I. Thermodynamic analysis of phase relations in the

Downloaded from https://academic.oup.com/petrology/article/49/2/239/1551155 by guest on 20 April 2024

system CaO–FeO–Fe_2O_3–Al_2O_3–SiO_2–H_2O–CO_2. *American Journal of Science* **280**, 907–941.

Bøggild, O. B. (1902). On ilvaite from Siorarsuit at Julianehaab, Greenland. *Meddelelser om Grønland* **25**, 43–90.

Bohse, H., Brooks, C. K. & Kunzendorf, H. (1971). *Field observations on the kakortokites of the Ilímaussaq intrusion, south Greenland, including mapping and analyses by portable X-ray fluorescence equipment for zirconium and niobium. Grønlands Geologiske Undersøgelse Rapport* **38**, 42 pp.

Boily, M. & Williams-Jones, A. E. (1994). The role of magmatic and hydrothermal processes in the chemical evolution of the Strange Lake plutonic complex, Québec–Labrador. *Contributions to Mineralogy and Petrology* **118**, 33–47.

Chacko, T., Riciputi, R., Cole, R. & Horita, J. (1999). A new technique for determining equilibrium hydrogen isotope fractionation factors using the ion microprobe: Application to the epidote–water system. *Geochimica et Cosmochimica Acta* **63**, 1–10.

Clayton, R. N. & Mayeda, T. K. (1963). The use of bromine pentafluoride in the extraction of oxygen from oxides and silicates for isotope analysis. *Geochimica et Cosmochimica Acta* **27**, 43–52.

Coulson, I. M. (1997). Post-magmatic alteration in eudialyte form the North Qôroq centre, South Greenland. *Mineralogical Magazine* **61**, 99–109.

Coulson, I. M. (2003). Evolution of the North Qôroq centre nepheline syenites, south Greenland: alkali–mafic silicates and the role of metasomatism. *Mineralogical Magazine* **67**, 873–892.

Deer, W.A., Howie, R.A. & Zussman, J. (1992). *An introduction to the rock forming minerals*. Pearson: Harlow, 712 pp.

Edgar, A. D. & Parker, L. M. (1974). Comparison of melting relationship of some plutonic and volcanic peralkaline undersaturated rocks. *Lithos* **7**, 263–273.

Einaudi, M. T. & Burt, D. M. (1982). Introduction—terminology, classification, and composition of skarn deposits. *Economic Geology* **77**, 745–754.

Einaudi, M. T., Meinert, L. D. & Newberry, R. J. (1981). Skarn deposits. *Economic Geology*, 75th Anniversary Volume, 317–391.

Emeleus, C. H. & Upton, B. G. J. (1976). The Gardar period in southern Greenland. In: Escher, A. & Watt, W. S. (eds) *Geology of Greenland. Grønlands Geologiske Undersøgelse*, pp. 153–181.

Engell, J., Hansen, J., Jensen, M., Kunzendorf, H. & Løvborg, L. (1971). *Beryllium mineralization in the Ilímaussaq intrusion, South Greenland, with description of a field beryllometer and chemical methods. Grønlands Geologikse Undersøgelse Rapport* **33**, 40 pp.

Ferguson, J. (1964). *Geology of the Ilímaussaq alkaline intrusion, South Greenland. Grønlands Geologiske Undersøgelse Bulletin* **39**, 82 pp.

Finch, A. (1995). Metasomatic overprinting by juvenile igneous fluids, Igdlerfigsalik, South Greenland. *Contributions to Mineralogy and Petrology* **122**, 11–24.

Friedman, I. & O'Neil, J. R. (1977). Compilation of stable isotope fractionation factors of geochemical interest. In: Fleischer, M. (ed.) *Data of Geochemistry. US Geological Survey, Professional Papers* **440-KK**, 12 pp.

Garde, A. A., Hamilton, M. A., Chadwick, B., Grocott, J. & McCaffrey, K. J. W. (2002). The Ketilidian orogen of South Greenland: geochronology, tectonics, magmatism, and fore-arc accretion during Palaeoproterozoic oblique convergence. *Canadian Journal of Earth Sciences* **39**, 765–793.

Gieré, R. & Sorensen, S. S. (2004). Allanite and other REE-rich epidote-group minerals. In: Liebscher, A. & Franz, G (eds) *Epidotes. Mineralogical Society of America, Reviews in Mineralogy and Geochemistry* **56**, pp. 431–493.

Giletti, B. J., Semet, M. P. & Yund, R. A. (1978). Studies in diffusion—III. Oxygen in feldspars: an ion microprobe determination. *Geochimica et Cosmochimica Acta* **42**, 45–57.

Gustafson, W. I. (1974). The stability of andradite, hedenbergite, and related minerals in the system Ca–Fe–Si–O–H. *Journal of Petrology* **15**, 455–496.

Halama, R., Wenzel, T., Upton, B. G. J., Siebel, W. & Markl, G. (2003). A geochemical and Sr–Nd–O isotopic study of the Proterozoic Eriksfjord Basalts, Gardar Province, South Greenland; reconstruction of an OIB signature in crustally contaminated rift-related basalts. *Mineralogical Magazine* **67**, 831–853.

Hansen, J. (1968). *A study of radioactive veins containing rare-earth minerals in the area surrounding the Ilímaussaq alkaline intrusion in South Greenland. Meddelelser om Grønland* **181**, 47 pp.

Holland, T. J. B. (1990). Activities of components in omphacitic solid solutions; an application of Landay theory of mixtures. *Contributions to Mineralogy and Petrology* **105**, 446–453.

Holland, T. J. B. & Powell, R. (1998). An internally consistent thermodynamic data set for phases of petrological interest. *Journal of Metamorphic Geology* **16**, 309–343.

Holland, T. J. B. & Powell, R. (2000). AX—Mineral activity calculations for thermobarometry. Computer program for Apple MacIntosh and PC. http://www.esc.cam.ac.uk/astaff/holland/ax.html.

Johnsen, O. & Gault, R. A. (1997). Chemical variation in eudialyte. *Neues Jahrbuch für Mineralogie, Abhandlungen* **171**, 215–237.

Johnson, J. W., Oelkers, E. H. & Helgeson, H. C. (1992). SUPCRT92: A software package for calculating the standard molal thermodynamic properties of minerals, gases, aqueous species, and reactions from 1 to 5000 bars and 0 to 1000°C. *Computers and Geosciences* **18**, 899–947.

Karup-Møller, S. (1978). *The ore minerals of the Ilímaussaq intrusion: their mode of occurrence and their conditions of formation. Bulletin Grønlands Geologiske Undersøgelse* **127**, 51 pp.

Khadem Allah, B., Fontane, F., Kadar, M., Monchoux, P. & Sørensen, H. (1998). Reactions between agpaitic nepheline syenitic melts and sedimentary carbonate rocks, exemplified by the Tamazeght Complex, Morocco. *Geochemistry International* **36**, 569–581.

Kieffer, S. W. (1982). Thermodynamics and lattice vibrations of minerals: 5. Applications to phase equilibria, isotopic fractionation and high-pressure thermodynamic properties. *Reviews of Geophysics and Space Physics* **20**, 827–849.

Konnerup-Madsen, J. & Rose-Hansen, J. (1982). Volatiles associated with alkaline igneous rift activity; fluid inclusions in the Ilímaussaq intrusion and the Gardar granitic complex (South Greenland). *Chemical Geology* **37**, 79–93.

Konnerup-Madsen, J. & Rose-Hansen, J. (1984). Composition and significance of fluid inclusions in the Ilimaussaq peralkaline granite, South Greenland. *Bulletin de Minéralogie* **107**, 317–326.

Kretz, R. (1983). Symbols for rock-forming minerals. *American Mineralogist* **68**, 277–279.

Krumrei, T. V., Villa, I. M., Marks, M. A. W. & Markl, G. (2006). A $^{40}Ar/^{39}Ar$ and U/Pb isotopic study of the Ilímaussaq complex, South Greenland: implications for the ^{40}K decay constant and for the duration of magmatic activity in a peralkaline complex. *Chemical Geology* **227**, 258–273.

Krumrei, T. V., Pernicka, E., Kaliwoda, M. & Markl, G. (2007). Volatiles in a peralkaline system: abiogenic hydrocarbons and F–Cl–Br systematics in the naujaite of the Ilímaussaq intrusion, South Greenland. *Lithos* **95**, 298–314.

Kunzendorf, H., Nyegaard, P. & Nielsen, B. L. (1982). *Distribution of characteristic elements in the radioactive rocks of the northern part of Kvanefjeld, Ilímaussaq instrusion, South Greenland. Rapport Grønlands Geologiske Undersøgelse* **109**, 32 pp.

Downloaded from https://academic.oup.com/petrology/article/49/2/239/1551155 by guest on 20 April 2024

Lager, G. A., Armbruster, T., Rotella, F. J. & Rossman, G. R. (1989). OH substitution in garnets: X-ray and neutron diffraction, infrared, and geometric-modeling studies. *American Mineralogist* **74**, 840–851.

Larsen, L. M. (1976). Clinopyroxenes and coexisting mafic minerals from the alkaline Ilímaussaq Intrusion, south Greenland: chemistry and petrological implications. *Journal of Petrology* **17**, 258–290.

Larsen, L. M. (1981). Chemistry of feldspars in the Ilímaussaq augite syenite with additional data on some other minerals. *Rapport Grønlands Geologiske Undersøgelse* **103**, 31–37.

Larsen, L. M. & Sørensen, H. (1987). The Ilímaussaq Intrusion—progressive crystallization and formation of layering in an agpaitic magma. In: Fitton, J. G. & Upton, B. G. J. (eds) *Alkaline Igneous Rocks. Geological Society, London, Special Publications* **20**, 473–488.

Leake, B. E., Woolley, A. R., Arps, C. E. S. *et al.* (1997). Nomenclature of amphiboles. Report of the Subcommittee on Amphiboles of the International Mineralogical Association Commission on New Minerals and Mineral Names. *European Journal of Mineralogy* **9**, 623–651.

Leake, B. E., Woolley, A. R., Birch, W. D. *et al.* (2004). Nomenclature of amphiboles: additions and revisions to the International Mineralogical Association's amphibole nomenclature. *European Journal of Mineralogy* **16**, 191–196.

Liou, J. G., Kim, H. S. & Maruyama, S. (1983). Prehnite–epidote equilibria and their petrologic applications. *Journal of Petrology* **24**, 321–342.

Lorenzen, L. (1881). Undersøgelse of nogle Mineralier i Sodalith-Syenite fra Julianehaabs Distrikt. *Meddelelser om Grønland* **2**, 43–79.

Markl, G. (2001*a*). A new type of silicate liquid immiscibility macroscopically visible in Proterozoic peralkaline rocks from Ilímaussaq, South Greenland. *Contributions to Mineralogy and Petrology* **141**, 458–472.

Markl, G. (2001*b*). Stability of Na–Be minerals in late-magmatic fluids of the Ilímaussaq alkaline complex. South Greenland. *Geology of Greenland Survey Bulletin* **190**, 145–158.

Markl, G. & Baumgartner, L. (2001). pH changes in late-magmatic peralkaline fluids. *Contributions to Mineralogy and Petrology* **144**, 331–346.

Markl, G., Marks, M., Schwinn, G. & Sommer, H. (2001). Phase equilibrium constraints on intensive crystallization parameters of the Ilímaussaq complex, South Greenland. *Journal of Petrology* **42**, 2231–2258.

Marks, M. & Markl, G. (2001). Fractionation and assimilation processes in the alkaline augite syenite unit of the Ilímaussaq Intrusion, South Greenland, as deduced from phase equilibria. *Journal of Petrology* **42**, 1947–1969.

Marks, M., Vennemann, T., Siebel, W. & Markl, G. (2003). Quantification of magmatic and hydrothermal processes in a peralkaline syenite–alkali granite complex based on textures, phase equilibria, and stable and radiogenic isotopes. *Journal of Petrology* **44**, 1247–1280.

Marks, M., Vennemann, T., Siebel, W. & Markl, G. (2004). Nd-, O-, and H-isotopic evidence for complex, closed-system fluid evolution of the peralkaline Ilímaussaq intrusion, South Greenland. *Geochimica et Cosmochimica Acta* **68**, 3379–3395.

Matsuhisa, Y., Goldsmith, J. R. & Clayton, R. N. (1979). Oxygen isotope fractionation in the system quartz–albite–anorthite–water. *Geochimica et Cosmochimica Acta* **43**, 1131–1140.

McDonough, W. F. & Sun, S. S (1995). The composition of the Earth. *Chemical Geology* **120**, 223–253.

Meinert, L. D., Dipple, G. M. & Nicolescu, S. (2005). World skarn deposits. *Economic Geology*, 100th anniversary volume, 299–336.

Metcalf-Johansen, J. (1983). Prehnite from the Ilímaussaq alkaline intrusion. *Mineralogical Magazine* **47**, 403–404.

Millero, F. J. (2004). Physicochemical controls on seawater. In: Elderfield, H., Holland, H. D. & Turekian, K. K. (eds) *Treatise on Geochemistry, Volume 6—The Oceans and Marine Geochemistry.* Amsterdam: Elsevier, pp. 1–21.

Müller-Lorch, D., Marks, M. A. W. & Markl, G. (2007). Na and K distribution in agpaitic pegmatites. *Lithos* **95**, 315–330.

Oelkers, E. H. & Helgeson, H. C. (1990). Triple-ion anions and polynuclear complexing in supercritical electrolyte solutions. *Geochimica et Cosmochimica Acta* **54**, 727–738.

Parsons, I., Mason, R. A., Becker, S. M. & Finch, A. A. (1991). Biotite equilibria and fluid circulation in the Klokken Intrusion. *Journal of Petrology* **32**, 1299–1333.

Paslick, C. R., Halliday, A. N., Davies, G. R., Mezger, K. & Upton, B. G. J. (1993). Timing of Proterozoic magmatism in the Gardar Province, southern Greenland. *Geological Society of America Bulletin* **105**, 272–278.

Pauly, H. & Bailey, J. C. (1999). *Genesis and evolution of the Ivigtut cryolite deposit, SW Greenland. Meddelelser om Grønland Geoscience* **37**, 60 pp.

Petersen, O. V., Micheelsen, H. I. & Leonardsen, E. S. (1995). Bavenite, $Ca_4Be_3Al[Si_9O_{25}(OH)_3]$, from the Ilímaussaq alkaline complex, South Greenland. *Neues Jahrbuch für Mineralogie, Monatshefte* **7**, 321–335.

Piotrowski, J. M. & Edgar, A. D. (1970). *Melting relations of undersaturated alkaline rocks from South Greenland. Meddelelser om Grønland* **181**, 62 pp.

Poulsen, V. (1964). *The sandstones of the Precambrian Eriksfjord Formation in Southern Greenland. Rapport Grønlands Geologiske Undersøgelse* **2**, 16 pp.

Qian, Y. & Guo, J. (1993). Study of hydrogen isotope equilibrium and kinetic fractionation in the ilvaite–water system. *Geochimica et Cosmochimica Acta* **57**, 3073–3082.

Rae, D. A., Coulson, I. M. & Chambers, A. D. (1996). Metasomatism in the North Qôroq centre, South Greenland: apatite chemistry and rare-earth element transport. *Mineralogical Magazine* **60**, 207–220.

Ranløv, J. & Dymek, R. F. (1991). Compositional zoning in hydrothermal aegirine from fenites in the Proterozoic Gardar Province, South Greenland. *European Journal of Mineralogy* **3**, 837–853.

Rossman, G. R. & Aines, R. D. (1986). Spectroscopy of a birefringent grossular from Asbestos, Quebec, Canada. *American Mineralogist* **71**, 779–780.

Rumble, D & Hoering, T. C. (1994). Analysis of oxygen and sulfur isotope ratios in oxide and sulfide minerals by spot heating with a carbon dioxide laser in a fluorine atmosphere. *Accounts of Chemical Research* **27**, 237–241.

Salvi, S. & Williams-Jones, A. E. (1990). The role of hydrothermal processes in the granite-hosted Zr, Y, REE deposit at Strange Lake, Quebec/Labrador: evidence from fluid inclusions. *Geochimica et Cosmochimica Acta* **54**, 2403–2418.

Salvi, S. & Williams-Jones, A. E. (1996). The role of hydrothermal processes in concentration high-field strength elements in the Strange Lake peralkaline complex, northeastern Canada. *Geochimica et Cosmochimica Acta* **60**, 1917–1932.

Salvi, S. & Williams-Jones, A. E. (2006). Alteration, HFSE mineralisation and hydrocarbon formation in peralkaline igneous systems: Insights from the Strange Lake Pluton, Canada. *Lithos* **91**, 19–34.

Salvi, S., Fontan, F., Monxhoux, P., Williams-Jones, A. E. & Moine, B. (2000). Hydrothermal mobilization of high field strength elements in alkaline igneous systems: evidence from the Tamazeght complex (Morocco). *Economic Geology* **95**, 559–676.

Savatenkov, V. M., Morozova, I. M. & Levsky, L. K. (2004). Behavior of the Sm–Nd, Rb–Sr, K–Ar, and U–Pb isotopic systems during alkaline metasomatism: Fenites in the outer-contact zone of

Downloaded from https://academic.oup.com/petrology/article/49/2/239/1551155 by guest on 20 April 2024

an ultramafic–alkaline intrusion. *Geochemistry International* **42**, 899–920.

Schönenberger, J., Marks, M., Wagner, T. & Markl, G. (2006). Fluid–rock interaction in autoliths of agpaitic nepheline syenites in the Ilímaussaq intrusion, South Greenland. *Lithos* **91**, 331–351.

Sharp, Z. D. (1990). A laser-based microanalytical method for the *in-situ* determination of oxygen isotope ratios of silicates and oxides. *Geochimica et Cosmochimica Acta* **54**, 1353–1357.

Sheppard, S. M. F. (1986). Characterization and isotopic variations in natural waters. In: Valley, J. W., Taylor, H. P., Jr & O'Neil, J. R. (eds) *Stable Isotopes. Mineralogical Society of America, Reviews in Mineralogy* **16**, 165–181.

Shimazaki, H. (1982). The Sasano hastingsite-bearing copper skarn deposit formed in aluminous sediment, at the Yoshioka mine, Japan. *Economic Geology* **77**, 868–876.

Shock, E. L., Oelkers, E. H., Johnson, J. W., Sverjensky, D. A. & Helgeson, H. C. (1992). Calculation of the thermodynamic properties of aqueous species at high pressures and temperatures. *Journal of the Chemical Society, Faraday Transactions* **88**, 803–950.

Shock, E. L., Sassani, D. C., Willis, M. & Sverjensky, D. A. (1997). Inorganic species in geological fluids: correlation among standard molal thermodynamic properties of aqueous ions and hydroxide complexes. *Geochimica et Cosmochimica Acta* **61**, 907–950.

Shvarov, Y. V. (1978). Minimization of the thermodynamic potential of an open chemical system. *Geochemistry International* **15**, 200–203.

Shvarov, Y. V. (1981). A general equilibrium criterion for an isobaric–isothermal model of a chemical system. *Geochemistry International* **18**, 38–45.

Shvarov, Y. V. & Bastrakov, E. N. (1999). *HCh: a software package for geochemical equilibrium modelling. User's Guide. Australian Geological Survey Organisation, Record* **1999/25**, 61 pp.

Sindern, S. & Kramm, U. (2002). Volume characteristics and element transfer of fenite aureoles: A case study from the Iivaara alkaline complex, Finland. *Lithos* **51**, 75–93.

Sobolev, V. S., Bazarova, T. Y., Shugurova, N. A., Bazarov, L. S., Dolgov, Y. A. & Sørensen, H. (1970). A preliminary examination of fluid inclusions in nepheline, sørensenite, tugtupiote and chkalovite from the Ilímaussaq alkaline intrusion, South Greenland. *Bulletin, Geological Survey of Greenland* **81**, 1–21.

Sood, M. K. & Edgar, A. D. (1970). *Melting relations of undersaturated alkaline rocks. Meddelelser om Grønland* **181**, 41.

Sørensen, H. (1962). *On the occurrence of streenstrupine in the Ilímaussaq massif, southwest Greenland. Meddelelser om Grønland* **167**, 251 pp.

Sørensen, H. (1969). Rhythmic igneous layering in peralkaline intrusions. *Lithos* **2**, 261–283.

Sørensen, H. (1992). Agpaitic nepheline syenites: a potential source of rare elements. *Applied Geochemistry* **7**, 417–427.

Sørensen, H. (1997). The agpaitic rocks—an overview. *Mineralogical Magazine* **61**, 485–498.

Sørensen, H. (2001). Brief introduction to the geology of the Ilímaussaq alkaline complex, South Greenland, and its exploration history. *Geology of Greenland Survey Bulletin* **190**, 7–24.

Sørensen, H. (2006). *The Ilímaussaq alkaline complex, South Greenland—an overview of 200 years of research and an outlook. Meddelelser om Grønland* **45**, 70 pp.

Sørensen, H. & Larsen, L. M. (2001). The hyper agpaitic stage in the evolution of the Ilímaussaq alkaline complex, South Greenland. In: Sørensen, H. (ed.) *The Ilímaussaq alkaline complex. South Greenland: status of mineralogical research with new results. Geology of Greenland Survey Bulletin* **190**, 83–94.

Sørensen, H., Rose-Hansen, J., Nielsen, B. L., Løvborg, L., Sørensen, E. & Lundgaard, T. (1974). The Uranium Deposit at Kvanefjeld, the Ilímaussaq Intrusion, South Greenland, Geology, Reserves and Beneficiation. *Geological Survey Greenland, Report* **60**, 1–54.

Sørensen, H., Bailey, J. C., Kogarko, L. N., Rose-Hansen, J. & Karup-Møller, S. (2003). Spheroidal structures in arfvedsonite lujavrite, Ilímaussaq alkaline complex, South Greenland—an example of macro-scale liquid immiscibility. *Lithos* **70**, 1–20.

Sørensen, H., Bohse, H. & Bailey, J. C. (2006). The origin and mode of emplacement of lujavrites in the Ilímaussaq alkaline complex, South Greenland. *Lithos* **91**, 286–300.

Stevenson, R., Upton, B. G. J. & Steenfelt, A. (1997). Crust–mantle interaction in the evolution of the Ilímaussaq Complex, South Greenland: Nd isotopic studies. *Lithos* **40**, 189–202.

Sverjensky, D. A., Shock, E. L. & Helgeson, H. C. (1997). Prediction of the thermodynamic properties of aqueous metal complexes to 1000° and 5 kb. *Geochimica et Cosmochimica Acta* **61**, 1359–1412.

Taylor, B. E. (1976). Origin and significance of C–O–H fluids in the formation of Ca–Fe–Si skarn, Osgood Mountains, Humboldt County, Nevada. PhD dissertation, Stanford University.

Taylor, H. P., Jr (1997). Water/rock interactions and the origin of H_2O in granitic batholiths. *Journal of the Geological Society, London* **133**, 509–558.

Taylor, H. P., Jr & Sheppard, S. M. F. (1986). Igneous rocks: I. Processes of isotopic fractionation and isotope systematics. In: Valley, J. W., Taylor, H. P., Jr & O'Neil, J. R. (eds) *Stable Isotopes in High Temperature Geological Processes. Mineralogical Society of America, Reviews in Mineralogy* **16**, 227–271.

Upton, B. G. J. & Emeleus, C. H. (1987). Mid-Proterozoic alkaline magmatism in southern Greenland: the Gardar province. In: Fitton, J. G. & Upton, B. G. J. (eds) *The Alkaline Rocks. Geological Society, London, Special Publications* **30**, 449–471.

Upton, B. G. J., Emeleus, C. H., Heaman, L. M., Goodenough, K. M. & Finch, A. A. (2003). Magmatism of the mid-Proterozoic Gardar Province, South Greenland: chronology, petrogenesis and geological setting. *Lithos* **68**, 43–65.

Ussing, N. V. (1912). *Geology of the country around Julianehaaab, Greenland. Meddelelser om Grønland*, **38**, 426 pp.

Valley, J. W., Essene, E. J. & Peacor, D. R. (1983). Fluorine-bearing garnets in Adirondack calc-silicates. *American Mineralogist* **68**, 444–448.

Valley, J. W., Kitchen, N., Kohn, M. J., Niendorf, C. R. & Spicuzza, M. (1995). UWG-2, a garnet standard for oxygen isotope ratios: Strategies for high precision and accuracy with laser heating. *Geochimica et Cosmochimica Acta* **59**, 5223–5231.

Veksler, I. V. (2004). Liquid immiscibility and its role at the magmatic–hydrothermal transition: A summary of experimental studies. *Chemical Geology* **210**, 7–31.

Vennemann, T. W. & O'Neil, L. R. (1993). A simple and inexpensive method of hydrogen isotope and water analyses of minerals and rocks based on zinc reagent. *Chemical Geology* **103**, 227–234.

Vennemann, T. W. & Smith, H. S. (1990). The rate and temperature of reaction of ClF_3 with silicate minerals, and their relevance to oxygen isotope analysis. *Chemical Geology (Isotope Geoscience Section)* **86**, 83–88.

Wegmann, C. E. (1938). *Geological investigations in southern Greenland. Part I. On the structural divisions of southern Greenland. Meddelelser om Grønland* **113**, 148 pp.

Zheng, Y. F. (1993*a*). Calculation of oxygen isotope fractionation in hydroxyl-bearing silicates. *Earth and Planetary Science Letters* **120**, 247–263.

Zheng, Y. F. (1993*b*). Calculation of oxygen isotope fractionation in anhydrous silicate minerals. *Geochimica et Cosmochimica Acta* **57**, 1079–1091.

Downloaded from https://academic.oup.com/petrology/article/49/2/239/1551155 by guest on 20 April 2024